Nanoscale

FEATURE ARTICLE

View Article Online
View Journal | View Issue

Cite this: *Nanoscale*, 2018, **10**, 6781

Physical stimuli-responsive liposomes and polymersomes as drug delivery vehicles based on phase transitions in the membrane

Yangwei Deng,[a,b] Jun Ling [b] and Min-Hui Li *[a,b,c]

This paper reviews liposomes with crystalline phase and polymersomes exhibiting crystalline and thermotropic liquid crystalline phases in the membrane. Intriguing morphologies of vesicles are described, including spherical, ellipsoidal and faceted vesicles, produced by a large variety of amphiphilic molecules and polymers with nematic phase, smectic phase or crystalline phase. It is highlighted how the phase transitions and the phase grain boundaries could be used ingeniously to destabilize the vesicular structure and to achieve cargo-release under the action of external stimulation. These liposomes and polymersomes are responsive to physical stimuli, such as temperature variation, shear stress, light illumination, and magnetic and electric fields. These stimuli-responsive properties make them promising candidates as new smart drug delivery systems.

Received 1st February 2018,
Accepted 9th March 2018

DOI: 10.1039/c8nr00923f

rsc.li/nanoscale

[a]*Chimie ParisTech, PSL University Paris, CNRS, Institut de Recherche de Chimie Paris, UMR8247, 11 rue Pierre et Marie Curie, 75005 Paris, France. E-mail: min-hui.li@chimieparistech.psl.eu*
[b]*MOE Key Laboratory of Macromolecular Synthesis and Functionalization, Department of Polymer Science and Engineering, Zhejiang University, 310027 Hangzhou, China*
[c]*Beijing Advanced Innovation Center for Soft Matter Science and Engineering, Beijing University of Chemical Technology, 15 North Third Ring Road, Chaoyang District, 100029 Beijing, China*

1. Introduction

Liposomes are vesicles composed of lipid bilayer membranes. Polymersomes are vesicles made of a bilayer membrane of amphiphilic block copolymers.[1,2] Compared to liposomes (with a 5 nm-thick membrane), polymersomes (with 10 to 30 nm-thick membranes) are more stable and robust, and to some extent they mimic better biological systems such as

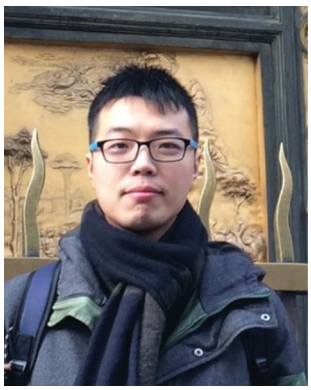

Yangwei Deng

Yangwei Deng obtained his B.S. from Zhejiang University, China, in 2013. Thereafter he started his Ph.D. research with Prof. Jun Ling at Zhejiang University. Between 2015 and 2017 he participated in a joint Ph.D. project supported by the China Scholarship Council, and performed research with Prof. Min-Hui Li at Chimie ParisTech (ENSCP), France. His research focuses on the synthesis and self-assembly of amphiphilic block copolymers.

Jun Ling

Jun Ling obtained his PhD degree from Zhejiang University, China, in 2002. He became a faculty member of the Department of Polymer Science and Engineering thereafter. In 2004, he was promoted to an associate professor. Between 2005 and 2007, he conducted research as a postdoc with Prof. Thieo Hogen-Esch in the University of Southern California, USA. In 2011, he was awarded the Alexander von Humboldt Research Fellowship for Experienced Researchers, and he worked in Prof. Axel H. E. Müller's group in the University of Bayreuth and in Johannes Gutenberg University at Mainz, Germany, in 2012 and 2013. His research mainly focuses on the living/controlled polymerization methodology, the synthesis of functional polymers, and molecular modelling.

living cells and viruses.[3] The PEGylated liposomes and polymersomes are considered to be excellent candidates for carriers of drugs and bioimaging agents.[4–8] On the one hand, targeted transport could be achieved by taking advantage of the many possibilities to end-functionalize lipids and copolymers.[4,9] On the other hand, the controlled release of therapeutic substances could be integrated through the use of lipids and copolymers with structures that respond to chemical stimuli (such as hydrolysis, oxidation or reduction reactions, and pH changes) or physical stimuli (such as temperature variation, shear stress, light illumination, and magnetic and electric fields).[10–14] Taking the example of polymersomes, the strategies with chemical stimuli use hydrophobic blocks that could be progressively degraded[15] or converted into hydrophilic moieties,[16,17] or use a cleavable linkage between hydrophobic and hydrophilic blocks.[18] Upon chemical stimulation, the vesicular structure is disrupted and the encapsulated substance released within time periods ranging from seconds to hours. However, in some applications, such as cancer treatment, a fast and programmed release of drugs or active substances at a precise site induced by a remote stimulus is desirable to minimize the damage caused by therapeutic agents to the surrounding healthy tissue. Although some chemical stimuli-responsive systems, like pH- and reduction-responsive ones, can respond within seconds or minutes, they require that the chemical environment be modified. These environmental modifications may not always be compatible with the drug targeting sites. In contrast, physical stimuli show obvious advantages because they can be applied remotely and precisely without any chemical environmental change. Upon physical stimuli, a rapid modification of structures of hydrophobic blocks at molecular and self-assembly levels will induce a fast leakage or bursting of polymersomes (from milliseconds to seconds). Therefore, in this paper, we will focus on physical stimuli-responsive systems, and discuss especially strategies making use of the phase transitions in the membrane of vesicles which are actuated by physical stimuli (temperature change, shear stress, light illumination, *etc.*). We will describe, in an integral way, the crystalline and liquid crystalline phases in the membrane of both liposomes and polymersomes, their effects on the vesicle morphologies and their intriguing stimuli-responsive properties that allow achieving cargo-release. One of these strategies has already led to the invention of a thermo-sensitive nano-drug (ThermoDox®) that is being evaluated in Phase III clinically, and good performances have been recorded in recent analyses for cancer treatment.[19,20] Other strategies are still in the stage of fundamental research, but show proof of concept with very promising potential for stimuli-responsive controlled release.[10–14,21–24]

This feature article will be organized into four sections: "2. Liposomes with crystalline phase", "3. Polymersomes with crystalline phase", "4. Liquid crystal polymersomes" and "5. Summary and outlook".

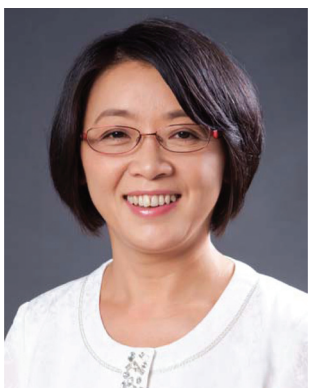

Min-Hui Li

Min-Hui Li received her B.S. (1986) and M.S. (1989) from Tsinghua University in Beijing, and her Ph.D. degree (1993) in Polymer Chemistry and Physical Chemistry from Pierre and Marie Curie University in Paris. She conducted her Ph.D. research in CEA Saclay and her postdoc research in the French Institute of Petroleum. She joined CNRS as a tenure researcher in 1994, and served in CRPP Bordeaux between 1994 and 1997 and in the Curie Institute in Paris between 1997 and 2014. She became a full professor in 2011. Since 2015, she has been working in Chimie ParisTech (ENSCP) in Paris. Her current research focuses on functional materials based on polymers and liquid crystals.

2. Liposomes with crystalline phase

It is well known that the membranes of liposomes can transform from an ordered state to a disordered state upon the increase of temperature. The transition temperature (melting temperature, T_m) is dependent on the molecular structures of lipids (hydrophobic alkyl chain structures and lengths, hydrophilic moieties *etc.*).[25–27] For example, DOPC (1,2-di-(9*Z*-octadecenoyl)-*sn-glycero*-3-phosphocholine) with two double bonds in the alkyl chains exhibits a T_m of −17 °C below room temperature (RT), while DPPC (1,2-dipalmitoyl-*sn-glycero*-3-phosphocholine) with entirely saturated chains shows a T_m of 42 °C above RT. The ordered state is often called the *gel* state and the disordered state the *liquid crystalline* state. Here we will call the ordered state the two-dimensional (2D) *crystalline* phase, and the disordered state the 2D *liquid* phase, in order to distinguish them from the thermotropic liquid crystalline phase exhibited in the membrane of polymersomes discussed further in this paper. The ordered state results from the crystalline properties of the hydrophobic alkyl chains of the lipids. Upon reaching T_m the crystalline domains melt and alkyl chains transform into an isotropic phase inside the 2D membrane.

The passive permeability of the bilayer membrane was found to be remarkably increased in the transition region and reaches the maximum at T_m.[28] Therefore liposomes with thermo-responsive release could be designed.[29–31] However, for liposomes composed of DPPC alone, the released amount of an encapsulated marker dye such as carboxyfluorescein (CF), was relatively small and the release is incomplete. The insertion of cholesterol[28,32] and coating with charged polymers[33] have been reported to controllably adjust the permeability by influencing the behaviour of lipids at the transition state. In the following examples, we will show other strategies to take advantage of the melting process of lipids. The defects and boundaries of the crystalline structures and

the pre-melting near boundary domains are used ingeniously to induce a sudden release upon temperature change or shear stress.

2.1. From thermo-responsive liposomes to ThermoDox®

In the late twentieth century, Needham reported the preparation of a thermo-sensitive liposome, by incorporating the single-tailed lysolipid MPPC (monopalmitoylphosphocholine: 1-palmitoyl-2-hydroxy-*sn-glycero*-3-phosphocholine) into the vesicle composed of the double-tailed phospholipid DPPC.[25,27] DPPC is a well-known phospholipid forming vesicles with a 2D crystalline phase in the membrane at room temperature (T_m = 42 °C), while its single-tail derivative MPPC forms only micelles. These could be explained by the geometric parameter, the packing parameter[34] $p = v/a_0 l$, where v is the volume of the hydrophobic part, l the length of the hydrophobic part, and a_0 the optimal area of the hydrophilic head. DPPC has a value of p between 1/2 and 1 ($1/2 < p < 1$), which allows the formation of enclosed bilayer membranes. In contrast, MPPC has a lower value of p (<1/3) because of the lower value of v, which leads to a spherical micelle. When MPPC was incorporated into DPPC at the ratio of 10 mol%, the mixture could still form stable vesicular structures, and the T_m of the membrane decreased from 42 °C (the peak value for pure DPPC, measured by DSC at 2 °C min^{-1}) to 41 °C (see Fig. 1). However, the highest release speed of liposomes made of a DPPC/MPPC mixture (DPPC : MPPC = 90 : 10) occurred at 39 °C, and at 41–42 °C the release had already been completed (see Fig. 1).

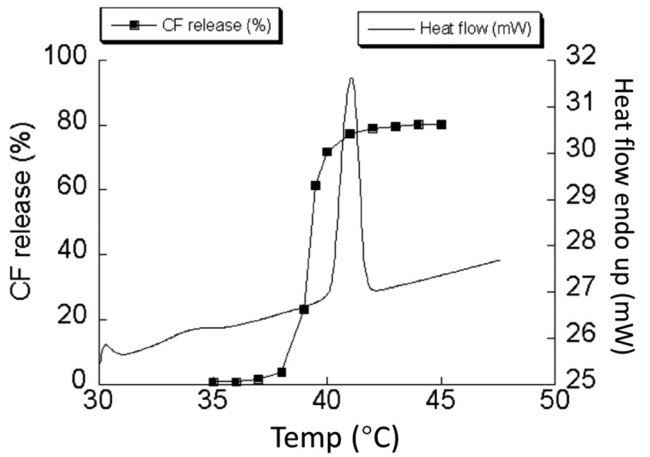

Fig. 1 Comparison between the differential scanning calorimetry of DPPC : MPPC = 90 : 10 liposomes and its cumulated release profile for CF release. Significant release occurs on the low temperature wing of the phase transition. Reproduced with permission from ref. 27. Copyright 2001, Elsevier.

It is reasonable to assume that MPPC molecules tend to assemble at the grain boundary of crystalline domains of DPPC under the spherical topology of vesicles and that they stabilize the holes if there are any because of their micelle-forming packing parameter (Fig. 2). A hypothetic illustration is a football-like structure (some kind of truncated icosahedron), where MPPC molecules form the edges and DPPC the faces. As the temperature increases, the pre-melting occurs first at the boundaries and causes the formation of enhanced defects, thus achieving significant release at a temperature where the lipids (in the faces) are still largely in the crystalline phase. The grain boundary pre-melting produces a rapid and enhanced release of contents over that observed in liposomes formed by pure DPPC lipids alone (Fig. 3).

The anti-cancer nano-drug ThermoDox® (Celsion Corp) is based on this thermo-sensitive liposome, encapsulating doxorubicin (DOX), a commonly used cancer drug.[19,35,36] ThermoDox® is used in combination with thermal therapies, such as radiofrequency thermal ablation (RFA),[20,36] microwave hyperthermia therapy,[37] and high-intensity focused ultrasound (HIFU) therapy.[38] ThermoDox® liposomes could concentrate in some cases at the tumor tissue as other nanomedicines did because of the EPR effect. Nevertheless, these thermo-sensitive nanomedicines are not dependent on the EPR effect when hyperthermia is applied prior to or quickly following drug administration. When $T \geq 40$ °C, DOX is released within seconds from the vesicles, and rapidly diffuses into the local tissue. Thermally triggered intravascular drug release improves

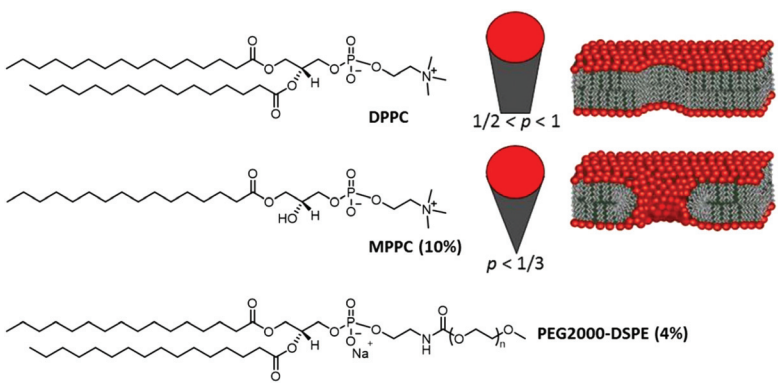

Fig. 2 Lipid composition of thermo-sensitive liposomes. Micelle-forming MPPC can stabilize the holes in the DPPC bilayer. The addition of PEG2000-DSPE offers a stealth layer of PEG to the liposome.

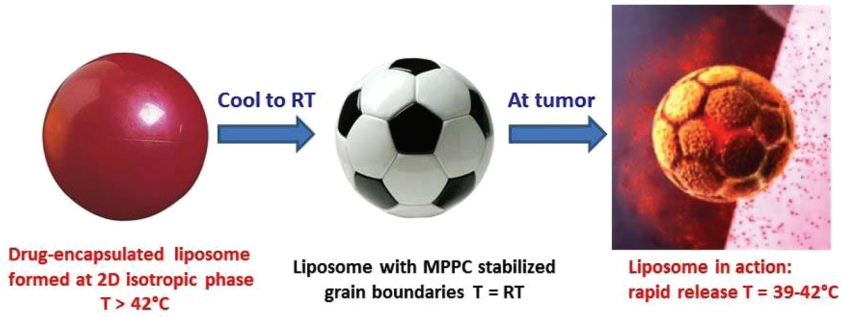

Fig. 3 Hypothetic illustration of ThermoDox® based on DPPC, MPPC (10%) and PEG2000-DSPE (4%) (the image of "liposome in action" comes from https://celsion.com/thermodox/).

drug penetration to reach more tumor cells than either with the EPR effect of PEGylated liposomes or with free drug.[39,40] Therapy combining ThermoDox® and RFA was established for patients with early-stage hepatocellular carcinoma.[20] A Phase III OPTIMA trial is in progress to confirm the increased survival with a standardized RFA dwell time of over 45 min.[41] In addition, therapy combining ThermoDox® and microwave hyperthermia for the treatment of chest wall breast cancer and therapy combining ThermoDox® and HIFU for primary liver cancer have also completed Phase I studies and have shown positive results.[42,43]

Since the first publication of Needham's thermo-sensitive liposomes,[25] numerous studies on other thermo-sensitive liposomes have been reported.[44] With a similar working mechanism, different liposomal formulations were developed for DOX delivery with further advantages, such as still faster drug release, enhanced anti-tumour effects,[45] longer circulation time,[46] *etc*. It is believed that the combination of thermo-sensitive nanomedicines like ThermoDox® with thermal therapy could revolutionize therapy in oncology.[47]

2.2. From faceted vesicles of catanionic surfactants to shear stress responsive liposomes

2.2.1. Catanionic faceted vesicles. Vesicles could be formed by various amphiphiles in addition to phospholipids, such as surfactants,[48] peptides,[49] ionic liquids,[50] supramolecular cyclodextrin,[51] *etc*. Among them, catanionic surfactants showed unique properties. Catanionic systems are a mixture of cationic and anionic surfactants (*e.g.*, fatty acid and cationic or amine components) and are known to produce a very wide range of self-assembled nano- and micro-structures.[52] When a cationic surfactant such as myristic acid ($C_{13}COOH$, $p < 1/3$) is mixed with an anionic surfactant such as cetyltrimethylammonium hydroxide (CTAOH, also $p < 1/3$), the strong reduction in area per head group due to electrostatic interactions induces the formation of molecular bilayers ($1/2 < p < 1$) at low concentrations. The two single chains of cationic and anionic surfactants act as double-tailed zwitterionic surfactants. By mixing the two surfactants $C_{13}COOH$ and CTAOH, salt-free catanionic systems were produced because the counter-ions were only H^+ and OH^- and no excess salt was formed.[53] The crucial parameter in these systems is the molar ratio (r) between the two species given by: r = [anionic surfactant]/[[anionic surfactant] + [cationic surfactant]], on which the morphology of various self-assemblies and the sign of the structural charge depend. In the case of the mixture of $C_{13}COOH$ and CTAOH, two peculiar ratios 1/3 (cationic CTAOH in excess) and 2/3 (anionic $C_{13}COOH$ in excess) are very interesting. For r = 1/3 nanodisks were present,[54] while for r close to 2/3 regular hollow icosahedra (faceted vesicles) were formed (Fig. 4a and b).[55] The ionic pair exhibits a phase transition from 2D crystalline to liquid phase ($T_m \sim$ 50–65 °C depending on the value of r). Zemb *et al.* studied the structural transformation of the catanionic vesicles of $C_{13}COOH$ and CTAOH in water (r in the range 0.5–0.75) upon temperature change. Spherical vesicles were first formed above T_m of ionic pairs. When the solution was

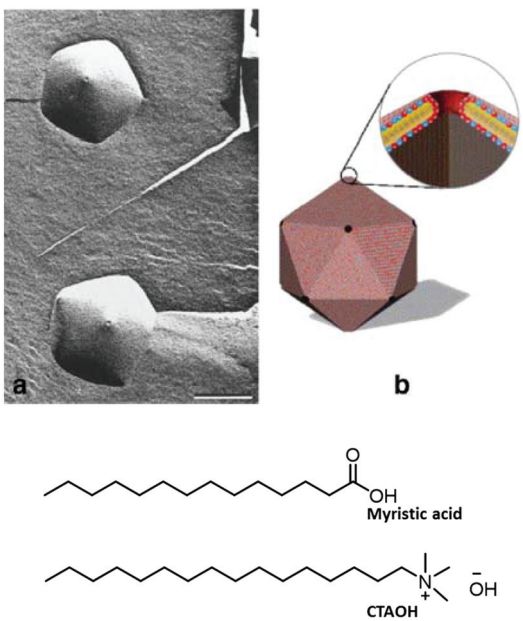

Fig. 4 Freeze facture image of the icosahedra (a) obtained from a mixture of myristic acid and cetyltrimethylammonium hydroxide (CTAOH) and the corresponding schematic (b). Scale bar = 250 nm. Reproduced with permission from ref. 55. Copyright 2001, Nature Publishing Group.

cooled down from 60 °C to room temperature, micron-sized icosahedra were formed. The transition of alkyl chains from 2D liquid to crystalline state was responsible for this morphological change. Upon crystallization, excess anionic surfactants accumulated on the edges or pores rather than being incorporated into crystalline bilayers. Fluorescence confocal microscopy directly showed the segregation of anionic components within the self-assemblies.[56] The observed shapes were consistently reproduced upon thermal cycling, demonstrating that the icosahedral shape corresponded to the existence of a local minimum of bending energy for faceted icosahedra when the optimal amount of excess segregated material (anionic components) was present.[56] Experimental results and simulations have also shown the possibility of obtaining various faceted structures with high rigidity.[57–63]

It has been expected that these faceted vesicles with a combination of wall rigidity and holes at vertices could be used for the encapsulation and controlled release of drugs or DNA, because they are probably more sensitive to mechanical stress than conventional spherical liposomes. However, the colloidal dispersion was highly stable only because there was no salt in these catanionic systems and the colloid presented a high osmotic pressure induced by unscreened electrostatic repulsions. In other words, catanionic faceted vesicles could only exist under salt-free conditions,[55,56] and would dissociate at the isotonic sodium chloride concentrations needed for drug delivery. Very interestingly, the team of Zumbuehl has proposed other lipidic systems that led effectively to shear stress sensitive non-spherical liposomes with promising potential for drug delivery.

2.2.2. Shear stress sensitive liposomes. To obtain non-spherical vesicles, lipid membranes need to have large bending moduli (*e.g.*, in a crystalline phase). Besides systems composed of natural phospholipids or catanionic surfactants with T_m > RT as discussed above, the crystalline feature of the membrane could also be introduced or enhanced by exchanging the ester bonds of natural phospholipids for artificial amides that stabilize the interfacial region through hydrogen bonds.[64–69] Among them, the symmetrical insertion of carbohydrate fatty amides at the 1- and 3-positions of glycerol and a residual phosphate ester at the 2-position gave the most exciting results.[64] An example of this kind of molecules, named Pad-PC-Pad (1,3-dipalmitamidopropan-2-yl 2-(trimethylammonio) ethyl phosphate), is an artificial amide homologue of DPPC (Fig. 5).

Pad-PC-Pad exhibits a melting temperature of T_m = 37 °C and forms vesicles with faceted shapes.[70,71] These vesicles are stable in a salt-containing buffer and under static conditions. Zumbuehl *et al.* showed, by using a cardiovascular model system, that drugs were preferentially released from the vesicles in constricted vessels (such as those found in atherosclerotic patients) where the shear stress was high (Fig. 6).[72] Their model system was based on polymer tubes and an external pump to represent shear stress in healthy and constricted vessels of the heart. This study suggested that such vesicles could be potentially used to treat cardiovascular diseases such as atherosclerosis in a targeted manner. When passing through a critically stenosed vessel, thrombolytic reagents could be released from the faceted vesicles as the wall shear stress increased significantly.[73] A study of preclinical safety tests showed that the Pad-PC-Pad vesicles had less or similar risk of complement activation-related pseudo-allergy, compared to FDA-approved liposomal drugs.[74]

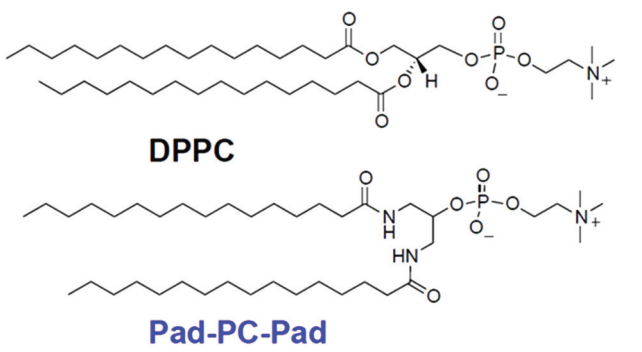

Fig. 5 Molecular structures of the natural lipid DPPC and its artificial homologue Pad-PC-Pad.

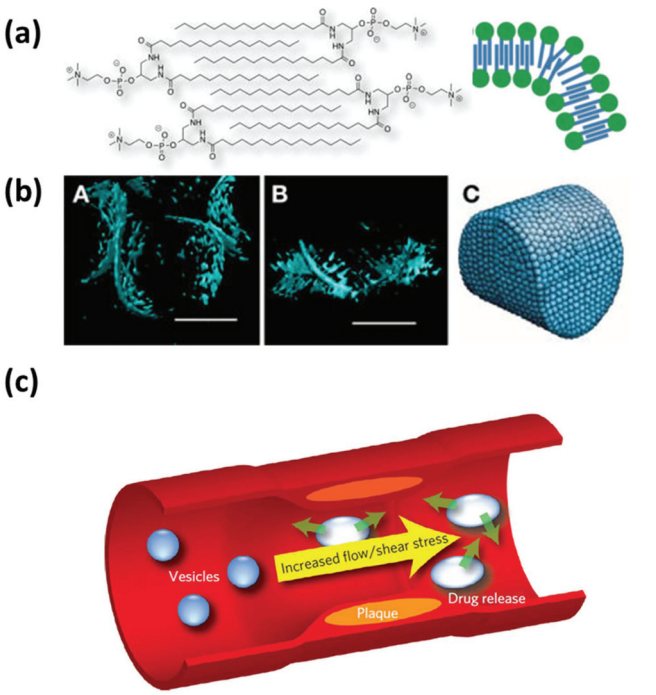

Fig. 6 (a) Arrangement of 1,3-diamidophospholipid Pad-PC-Pad inside the vesicle membrane. (b) A faceted Pad-PC-Pad vesicle by cryo-tomography. Top (A) and side (B) views. The artist's view in C shows the special D form that the vesicle may develop. The scale bars are 50 nm. (c) Nanocontainers liberate an active drug at the critically stenosed vessel because of the significantly increased wall shear stress. Reproduced with permission from ref. 70–72. Copyright 2015 and 2016, American Chemical Society, Copyright 2012, Nature Publishing Group.

In order to understand how the molecules of Pad-PC-Pad form faceted vesicles, studies on monolayer[75] and bilayer[71] properties of 1,3-diamidophospholipids were conducted. It was revealed that Pad-PC-Pad molecules took a unique interdigitated arrangement inside the bilayer membrane, where the two opposing leaflets interdigitated completely on forming the layer with thickness comparable to the length of a single phospholipid acyl chain (Fig. 6a).[70] The dense arrangement of lipids caused the lack of spontaneous curvature for the bilayer. Being forced to close into a vesicular structure, the Pad-PC-Pad bilayer formed faceted vesicles with the membrane broken (Fig. 6b). These defects were then responsible for the shear stress sensitivity, because preferential breaking points should be located along these defects when shear stresses are increased (Fig. 6c).

In a recent study published in 2017, Zumbuehl *et al.* reported another diamidophospholipid, Pad-Pad-PC, with the insertion of carbohydrate fatty amides at the 1- and 2-positions of glycerol and a residual phosphate ester at the 3-position, which also self-assembled into a faceted structure.[76] Different from Pad-PC-Pad, Pad-Pad-PC molecules pack into an exceptionally tight bilayer on cooling down below T_m, and the vesicles relax into a cuboid that maximizes flat faces and minimizes defect lines.

3. Polymersomes with crystalline phase

Due to the high molecular weight of polymers, polymersomes are much more stable, more robust and in most cases less permeable than liposomes.[1,77] Polymersomes are considered to be an advantageous alternative for drug encapsulation and delivery.[78] The glassy or ordered state of the polymer offers additional stability to the membrane of polymersomes. We will discuss first several examples of polymersomes with crystalline membranes.

3.1. Crystalline polymersomes self-assembled from block copolymers

The first example is a polymersome composed of a star-block copolymer $[PEO_{50}$-*b*-$PFDMS_{35}]_4$ with four arms (Fig. 7) reported by Schacher *et al.* Each arm of $[PEO_{50}$-*b*-$PFDMS_{35}]_4$ consists of an inner block of poly(ethylene oxide) (PEO) and a semi-crystalline outer block of poly(ferrocenyldimethylsilane) (PFDMS). The polymersomes were formed by the nanoprecipitation method with THF/ethanol as co-solvents (polymersomes dispersed in water could be obtained by dialysis first against ethanol and then against water).[79] Schacher *et al.* have shown that the addition rate of the selective solvent ethanol to the polymer solution in THF had a significant influence on the final morphology. A rather rapid precipitation was observed when ethanol was added for periods of 20 min or longer to obtain THF/ethanol (v/v) = 1/1, whereas stable vesicle dispersions were obtained for addition times of less than 15 min. The authors explained that in the last case the self-assembly

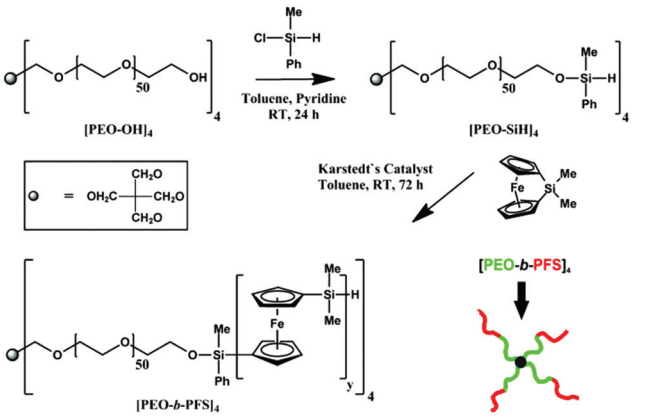

Fig. 7 Synthesis and structure of the copolymer [PEO-*b*-PFDMS]$_4$. Reproduced with permission from ref. 79. Copyright 2012, Wiley-VCH.

process proceeded in a sufficiently fast manner in the early stages to prevent extensive crystallization of the PFDMS and to favour vesicle formation. However, once the capsules have been formed, crystallization of the PFDMS domains induced rigidity, which was beneficial to their stability. They also demonstrated the stimuli-responsive degradation of polymersomes by incorporating inside the vesicles a photo-acid generator, 2-(4-methoxystyryl)-4,6-bis-(trichloromethyl)-1,3,5-triazine (PAG). Upon UV irradiation, PAG was decomposed and HCl was generated. HCl then induced the decomposition of PFDMS, and resulted in the degradation of the vesicles.

Another example of crystalline polymersomes is poly(ethylene oxide)-*b*-poly(ε-caprolactone) (PEO-*b*-PCL), where the hydrophobic polymer PCL is semi-crystalline in the pure state (T_m = 60 °C). Discher *et al.* have shown that the crystallization of PCL will result in leaky polymersomes.[80] Rehydration of polymer films of PEO2000-*b*-PCL13500 (2000 and 13 500 Da are the molecular weights M_n) at 60 °C yielded larger, smooth and round vesicles (Fig. 8A). Vesicles made in a sucrose solution and visualized in glucose appeared phase dark due to the refractive difference between inner sucrose and outer glucose solutions (Fig. 8A). Upon cooling to 25 °C, the vesicles not only appeared to be rough and irregular in shape but also lost the phase dark contrast. Membrane roughening is associated with dislocation defects in crystalline membranes.[81] Cracks or holes in crystalline membranes are responsible for the increase in membrane permeability that explains the sucrose release from polymersomes (Fig. 8B).

Our groups have also reported the self-assembly of PCL-based amphiphilic block copolymers.[82] We have synthesized the triblock copolymers polysarcosine-*b*-poly(ε-caprolactone)-*b*-polysarcosine (PSar-*b*-PCL-*b*-PSar) (Fig. 9), where the hydrophilic block is polysarcosine (PSar) instead of PEO. Through the nanoprecipitation method with co-solvents of DMF/water at room temperature, only large unilamellar sheets and nanofibers were formed by $PSar_{16}$-*b*-PCL_{40}-*b*-$PSar_{16}$ (16 and 40 are the degrees of polymerization DP$_n$; M_n = 4560 Da for PCL_{40} and M_n = 1140 Da for $PSar_{16}$). A thermal treatment by heating

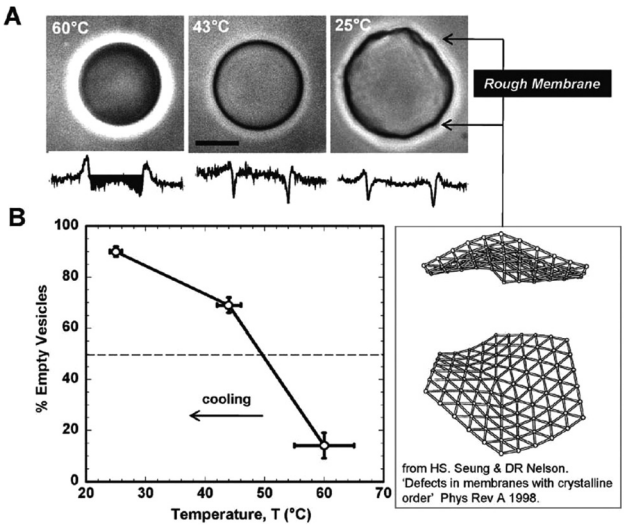

Fig. 8 Crystalline polymersomes based on PEO-*b*-PCL. Rigidity of CL membranes. (A) Representative phase contrast image of PEO2000-*b*-PCL13500 vesicles imaged after equilibrating at 60, 43, and 25 °C. The phase dark image shown in the left panel represents the retention of sucrose within vesicles at 60 °C. The model of a crystalline membrane roughened by dislocation defects is from Seung and Nelson.[81] (B) Proportion of empty vesicles as a function of temperature. Reproduced with permission from ref. 80. Copyright 2010, American Chemical Society.

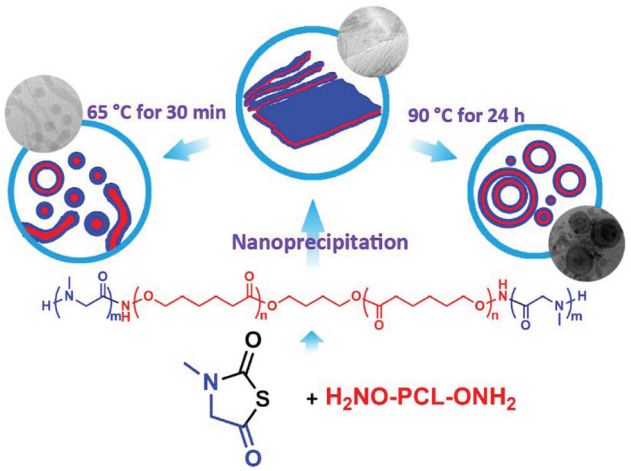

Fig. 9 Synthesis and self-assembling of the block copolymer PSar-PCL-PSar into polymersomes.[82] Copyright 2015, American Chemical Society.

the aqueous suspensions to 65 °C (higher than PCL melting point) transformed the lamellae and fibrous structures into worm-like cylinders, spheres and a few polymersomes. However, heating the initial aqueous suspension of nanoprecipitation to 90 °C led to a number of polymersomes. It suggested that the crystallization of the hydrophobic PCL core favoured the formation of rigid assemblies and low-curvature lamella at room temperature. By melting the crystalline phase and increasing the membrane flexibility, heating treatment facilitated vesicle formation. This work suggested that the formation of PSar-*b*-PCL-*b*-PSar polymersomes did not proceed from mechanism I, as proposed in the literature,[83] where amphiphilic block copolymers rapidly self-assembled into small spherical micelles, which then slowly evolved into cylindrical micelles and open disc-like micelles (lamellae) by collision, and finally lamellae closed into vesicles. Here the vesicular structures were more likely formed through mechanism II, where water diffused into bigger and complex spherical micelles (spherical particles) upon PCL melting, and lowered their bending energy by increasing the radius of curvature, thereby forming a hydrophilic cavity.[84]

Other authors used substituted amorphous-phase-forming polycaprolactone derivatives[85,86] in the copolymer structures, to avoid the crystallization of the membrane and to promote the polymersome formation.

The biodegradable poly(trimethylene carbonate) (PTMC) is another example of crystalline polymers. PTMC with molecular weights ranging from 1000 to 12 000 Da exhibit T_m close to the body temperature.[87] Lecommandoux and his colleagues have reported polymersomes made of poly(trimethylene carbonate)-*b*-poly(L-glutamic acid) (PTMC-*b*-PGA).[21] Vesicles were obtained by direct dissolution or nanoprecipitation, and the size of vesicles depended on the preparation conditions.[88] The authors showed that the crystalline phase of PTMC blocks was preserved in the membrane of vesicles of diameters ranging from 250 nm to 5 μm, using DSC ($T_m \sim 34$ °C measured) and polarizing optical microscopy (Fig. 10).[88] Then they reported the thermo-responsive release of DOX encapsulated in PTMC-based polymersomes.[89–91] For example, for PTMC-*b*-PGA vesicles encapsulating DOX at a loading content of 34 wt%,[89] they showed a strong temperature dependence of the kinetics and amount of drug release. The plateau values of DOX release at 5 °C, 20 °C, 37 °C and 45 °C were found, respectively, to be equal to 5%, 30%, 60% and 85% of the initial DOX load in the vesicles. It was suggested that this thermo-sensitivity resulted from the semi-crystalline nature of the PTMC blocks inside membranes. This example is reminiscent of the thermo-responsive liposomes firstly discussed in this paper. As the polymer membrane is thicker and more resilient, it is possible to incorporate inorganic nanoparticles such as ultrasmall superparamagnetic iron oxide (USPIO) inside the membrane. Lecommandoux's group utilized the well-known hyperthermia effect of USPIOs under an oscillating magnetic field to introduce the local temperature increase in the membranes of DOX/USPIO-encapsulated PTMC-*b*-PGA vesicles. The drug release rate was indeed enhanced two times upon the application of a radio frequency (RF) oscillating magnetic field.[90] This system presents a multifunctional polymersome that can combine imaging (here MRI) and therapy as theranostic systems.

A similar study was reported by Holder's group on the self-assembly of PEO-*b*-(PODMA-*co*-PDSMA),[92] a block copolymer with a random copolymer, poly(octadecyl methacrylate)-*co*-poly(docosyl methacrylate) (PODMA-*co*-PDSMA), as the hydrophobic block. PODMA has long linear alkyl chains ($C_{18}H_{37}$–) as

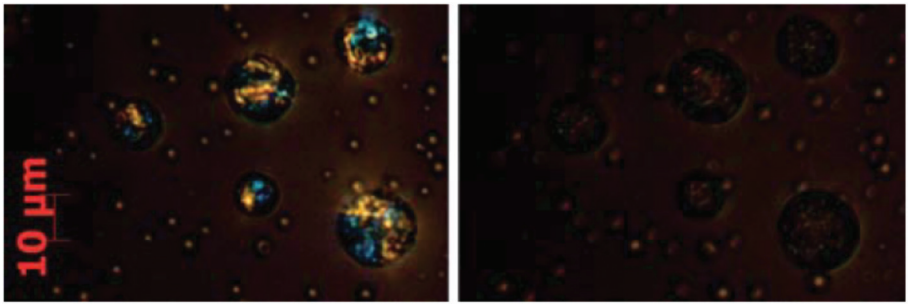

Fig. 10 PTMC-*b*-PGA vesicles are heated from 25 °C (left) to 40 °C (right). Upon heating, the disappearance of birefringence of the crystalline phase observed with optical microscopy under polarized light shows the phase transition. Reproduced with permission from ref. 21. Copyright 2010, Royal Society of Chemistry.

side groups, while PDSMA has shorter linear side groups ($C_{12}H_{25}$–). By varying the ratio of ODMA to DSMA, a series of copolymers were obtained and could assemble into polymersomes with bicontinuous and multilamellar morphologies. These aggregates displayed melting transitions in the range of 23.4 to 41.1 °C depending on the ODMA/DSMA ratio. An analysis of the rate of release of encapsulated ibuprofen demonstrated the close relationship between the release rate and the crystalline degree of the polymersome. A significantly enhanced release rate was found upon the melting of crystals in the membrane.

3.2. Crystalsomes made of crystalline homopolymers

All the crystalline polymersomes discussed above are made of amphiphilic block copolymers, where the membranes are semi-crystalline. Capsules with better structured crystalline (single crystal-like) phases were reported by C. Y. Li's group. These non-conventional polymersomes demonstrated an increase of two to three orders of magnitude in the bending modulus when compared to conventional polymersomes.[93] They used a miniemulsion crystallization method to grow nanoscale polymer single crystal-like capsules (Fig. 11), named crystalsomes. Using poly(L-lactic acid) (PLLA) as the model polymer, this group showed that the curved water/*p*-xylene interface formed by the miniemulsion process could guide the growth of PLLA single crystals. Crystalsomes have been formed with sizes ranging from 148 nm to over 1 μm and a thickness of 22.5 nm corresponding to the thickness of two layers of PLLA single lamella. Their membrane has a unique structure of homopolymer lamellar crystals (Fig. 11b), which is very different from that of the bilayer of amphiphilic polymers. Polymer crystals in a curved space/interface have to splay their chains from the inner layer to the outer layer to compensate for the curved geometry. Large defects or even amorphous polymer chains should be excluded to the outer layer, serving as 'wedges' to facilitate chain packing. Small defects such as vacancies tend to be located near the inner layer. This packing was feasible here because the crystalsome was formed *via* a nucleation–slow growth process and the defects had sufficient time to arrange and to accommodate the curved space at the liquid/liquid interface. Recently, C. Y. Li's group extended the crystalsome preparation method to polyethylene (PE), and obtained PE crystalsomes with high stability and robustness.[94] Moreover, hierarchical porous crystalsomes were prepared by a deep quenching process. These robust crystalsomes will be a promising system for drug delivery if structure tuning is introduced.

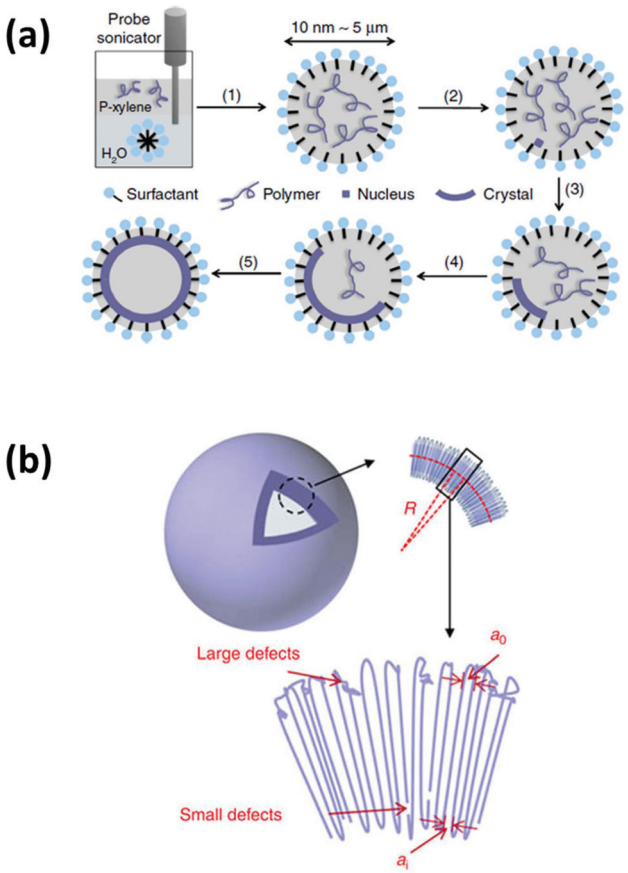

Fig. 11 (a) Schematic representation of the fabrication process of crystalsomes. (1) Emulsification; (2) quench to the crystallization temperature; and (3–5) different stages of crystal growth. (b) Schematic representation of a typical crystalsome and its defect distribution indicated by red arrows. Reproduced with permission from ref. 93. Copyright 2016, Nature Publishing Group.

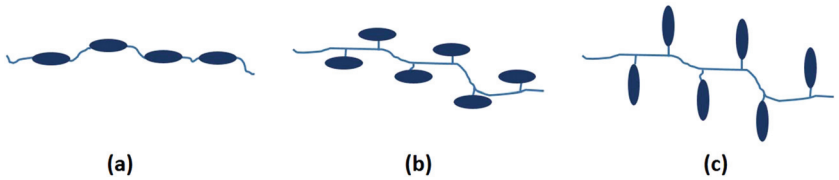

Fig. 12 (a) Main-chain LC polymer, (b) side-on side-chain LC polymer and (c) end-on side-chain LC polymer. The small elongated ellipsoid represents the rod-like mesogen.

Indeed, Landfester and her colleagues reported the control of the crystallization of crystalsomes to achieve controlled release.[95] They employed the miniemulsion method to obtain semi-crystalline polyurea polymersomes. In their work the polymer was synthesized *in situ* during capsule formation. An inverse miniemulsion was first formed with the aqueous core containing diamine, the surfactant and the cargo. As the diisocyanate was added to the system, the polycondensation was initiated at the water/oil interface. Crystalsomes with various thicknesses were obtained by controlling the amount of monomers during the synthesis. According to the DSC and XRD results, the melting temperature and the degree of crystallinity increased with the increase of the thickness. To further examine the influence of crystallinity, two kinds of diamines, methylpropane-1,3-diamine (MPDA) and diaminebutane (DAB), which have the same molecular weight but different atom arrangements (branched for MPDA and linear for DAB), were utilized, respectively, in the synthesis. For a comparable thickness, crystalsomes made from MPDA were found to have a lower degree of crystallinity than that of crystalsomes made from DAB. As a result, MPDA crystalsomes showed an obviously faster cargo release than DAB crystalsomes, confirming that the permeability of the crystalsome depends strongly on the degree of crystallinity. This research sheds light on the development of crystalsomes with a tuneable drug-release capability.

4. Liquid crystal polymersomes

Liquid crystalline (or liquid crystal (LC)) phases are mesomorphic phases (mesophases) situated between a solid crystalline phase and the liquid isotropic phase. LC molecules (also called mesogens) exhibit some orientational and positional orders similar to (but lower than) those of crystalline phases; meanwhile, they present some fluidity similar to (but lower than) that of isotropic liquids. Two major LC phases are the nematic phase and the smectic phase. In the nemectic phase (N), the molecules have no positional order, but self-align to have long-range orientational order with their long axes roughly parallel. The cholesteric phase (N*) is a chiral variant of the nematic phase, where the molecules twist along an axis perpendicular to the molecular long axes because of the presence of a chiral centre. In the smectic phase (Sm), the molecules are organized into well-defined layers that can slide over one another, while within the layers the molecules are 2D nematic-like or crystal-like depending on the smectic variety. The simplest smectic phase is the smectic A (SmA) phase where the molecules are parallel to the layer normal, but without positional order within the layer. Liquid crystal polymers combine the orientational ordering properties of LC systems and the viscoelastic properties of polymers. Using the LC polymer as the hydrophobic block of amphiphilic copolymers, it is then possible to form mesomorphic phases inside the vesicle membrane to give rise to polymersomes with unique structures and properties. It is well known that liquid crystal systems excel as responsive systems and could respond to multiple stimuli including temperature variation, light illumination, and electric and magnetic fields. If this responsiveness could be retained in the liquid crystal membrane, liquid crystal polymersomes could be developed as stimuli-responsive smart polymersomes, as detailed in the following subsections.

The structural diversity of LC polymers is either introduced by different mesogens, by different polymer backbones or by different methods of connecting the mesogens to the polymer chain. According to the method of connecting the mesogens, there are side-on and end-on side-chain LC polymers and main-chain LC polymers (Fig. 12). The mesogens can be simply thermotropic or both thermotropic and photo-sensitive (*e.g.*, with azobenzene group) for their responsive properties (Fig. 13). Meanwhile, they can be nematic, smectic or cholesteric for their mesophase structures (Fig. 13). Polyacrylate and polymethacrylate are the most common LC polymer backbones synthesized, for example, by atom transfer radical polymerization (Fig. 13a, PEG-*b*-PA444, PEG-*b*-PMAazo444, PEG-*b*-PAChol and PEG-*b*-PA6ester1).[96–100] Other backbones based on cyclopropane LC monomer (see Fig. 13b, PEG-*b*-PCpEChol) by anionic polymerization[101] or based on PEG-*b*-PBD (90% of 1,2-olefin) by post-grafting of mesogens (see Fig. 13b, PEG-*b*-P(PBD-*g*-Chol))[102] are also used. Our group in Paris is a pioneer group in the development of liquid crystal polymersomes and we have focused on side-chain LC copolymers as shown in Fig. 13.[96–102] There are also a few other authors reporting LC polymersomes.[103–105] They used cyclic amphiphilic block copolymers with LC blocks bearing cholesterol mesogen as the side-chain[103] or linear amphiphilic block copolymers with hydrophobic blocks bearing perylene as the side-chain.[104] There is also one example of polymersomes made of main-chain LC copolymers.[105]

4.1. Polymersomes with main-chain LC polymers

Tezuka and coworkers synthesized linear triblock and cyclic diblock copolymers composed of hydrophilic poly(acrylic acid)

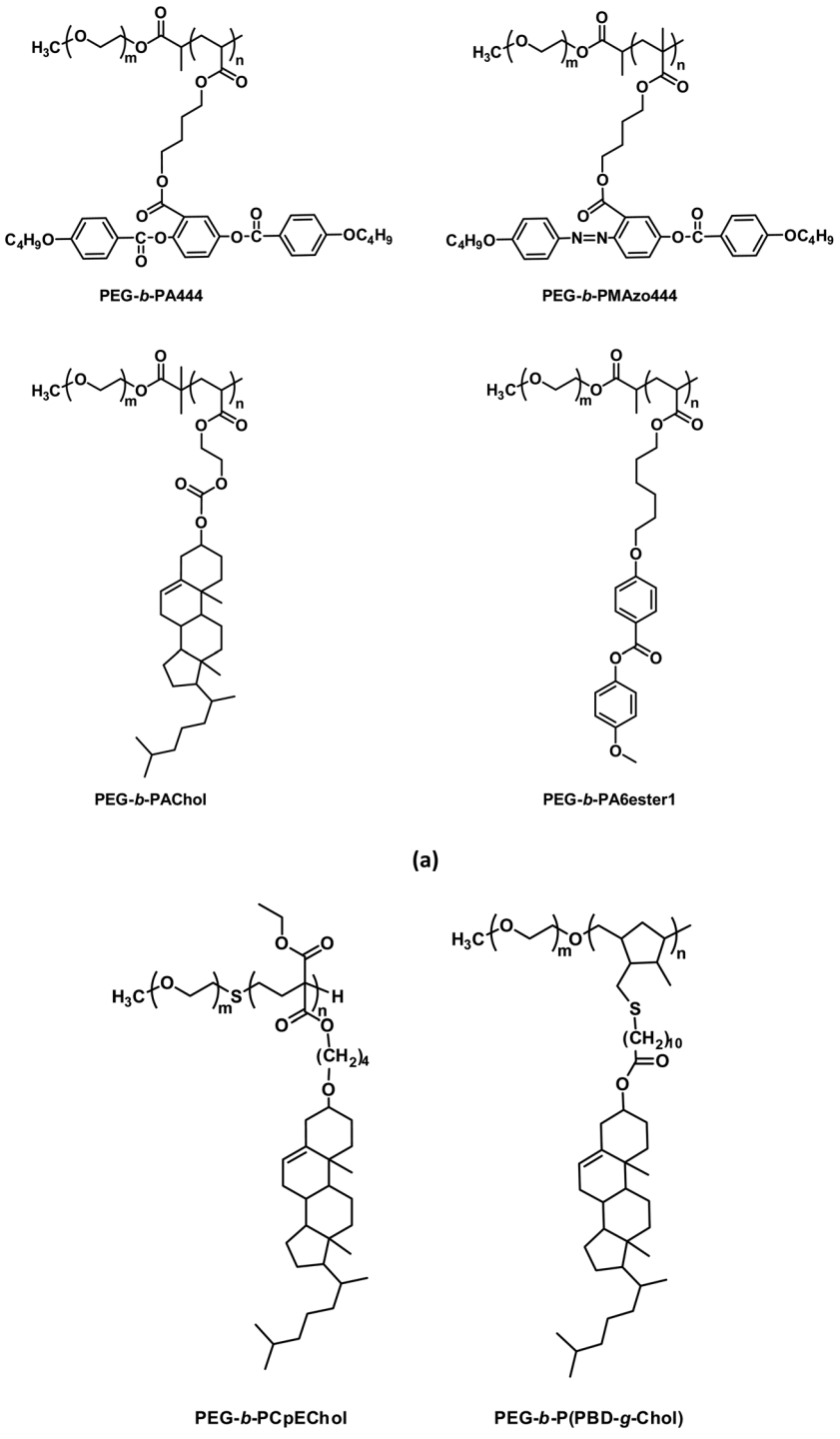

Fig. 13 Chemical structures of LC amphiphilic diblock copolymers: (a) synthesized by typical ATRP polymerization; (b) synthesized by other methods. PEG-*b*-PA444 has a thermotropic nematic LC block, and PEG-*b*-PMAzo444 a thermotropic and photo-sensitive LC block. PEG-*b*-PAChol, PEG-*b*-PA6ester1, PEG-*b*-PCpEChol and PEG-*b*-P(PBD-*g*-Chol) present thermotropic smectic LC blocks.

(AA) and hydrophobic poly(3-methylpentamethylene-4,4-bibenzoate) (BB) segments ($AA_{25}BB_{14}AA_{25}$ and cyclic $AA_{51}BB_{18}$) (Fig. 14).[105] These amphiphilic block copolymers were self-assembled in water to form vesicles or cylindrical micelles depending on the nanoprecipitation conditions. Fig. 15 shows TEM images of the polymersomes. The detailed LC structures and properties of the membrane are unfortunately not discussed. However, the authors have studied the response of

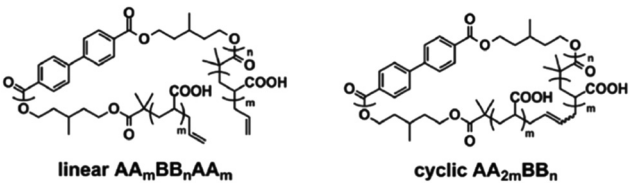

Fig. 14 Chemical structures of main-chain LC amphiphilic copolymers. Reproduced with permission from ref. 105. Copyright 2015, Royal Society of Chemistry.

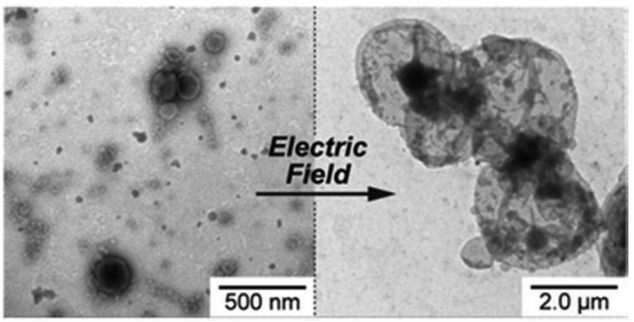

Fig. 15 TEM images of self-assembled structures of cyclic poly(acrylic acid)$_{51}$-poly(3-methylpentamethylene-4,4′-bibenzoate)$_{18}$ (cyclic $AA_{51}BB_{18}$) before (left) and after (right) the application of an electric field (E) of 1.5 V mm^{-1} for 2 min. Reproduced with permission from ref. 105. Copyright 2015, Royal Society of Chemistry.

these polymersomes to an electric field. They demonstrated that the nanoscale vesicles turned into micrometer-scale vesicles under an electric field. The transition was likely due to the reorganization of the LC segments in the bilayer, since when replacing BB parts with polystyrene (St) segments, the nanostructure formed by AA-St-AA copolymers did not show any response to the electric field.

4.2. Nematic polymersomes and photo-responsive LC polymersomes

Nematic side-on LC copolymers PEG-*b*-PA444 and PEG-*b*-PMAazo444 (Fig. 13) with appropriate hydrophilic/hydrophobic weight ratios (*e.g.*, from 40/60 to 19/81 for PEG-*b*-PA444) could form well-structured unilamellar spherical polymersomes using the nanoprecipitation method.[96,98] Fig. 16 shows examples of their cryo-electron micrographs (cryo-EM). The size of the observed vesicles is rather heterogeneous. Nevertheless, the membrane thickness is homogeneous: 10–11 nm for vesicles of PEG$_{45}$-*b*-PA444$_7$ and 14–15 nm for vesicles of PEG$_{45}$-*b*-PMAazo444$_{12}$ as measured by cryo-EM for their hydrophobic part. The thermotropic nematic nature of the membrane was confirmed by analysing the polymersome dispersions in water with high sensitivity differential scanning calorimetry (N-DSC).[106] A glass transition temperature (T_g) and a nematic–isotropic transition (T_{NI}) of the LC block are clearly observed in both PEG-*b*-PA444 and PEG-*b*-PMAazo444 polymersomes (see Fig. 17). The membrane is in a glassy nematic state at room temperature. The thickness of the nematic membrane corresponds to (and slightly higher than) twice the length of the stretched backbone of the hydrophobic block (stretched length of 4.4 nm for PA444 and 5.6 nm for PMAazo444). This means that the nematic LC backbones are stretched and present an elongated conformation along the normal of the membrane (see Fig. 18a).[107,108] Previous studies of chain conformation of side-on nematic polymers[107,108] have shown that the side-on nematic polymers undergo conformational changes from an elongated to a spherical shape at the T_{NI} transition. The obvious effect of this conformational change is the size contraction along the orientation direction of mesogens and the polymer backbone. This conformational change has been used to make LC polymer actuators either triggered by temperature change[109] or by UV illumination *via trans–cis* photo-isomerisation of azo-mesogen[110] (see Fig. 18b). In nematic polymersomes, this conformational change has been used to trigger vesicle opening by UV illumination.

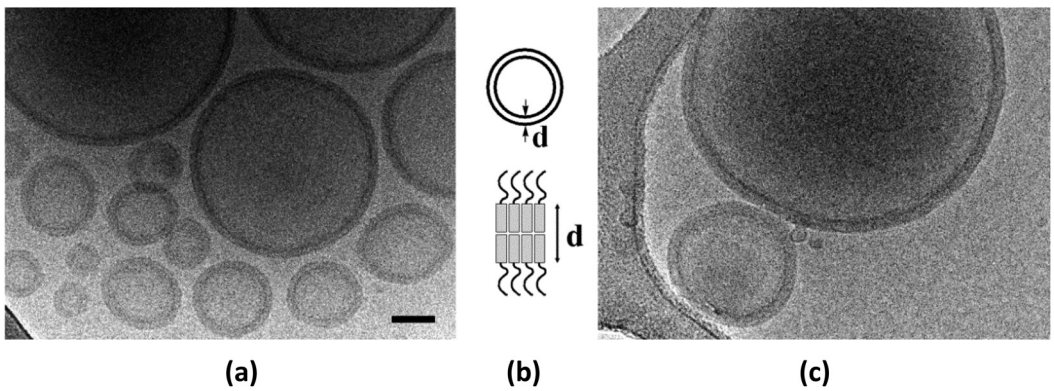

Fig. 16 Cryo-EM images of vesicles formed in water by PEG$_{45}$-*b*-PA444$_7$ (a) and PEG$_{45}$-*b*-PMAazo444$_{12}$ (c). The scale bar of (a) is 50 nm and the scale is the same for (c). The mean lamellar thickness d is 10–11 nm for PEG$_{45}$-*b*-PA444$_7$ and 14–15 nm for PEG$_{45}$-*b*-PMAazo444$_{12}$. (b) Schematic representation of diblock copolymers with a bilayer structure in the membrane (the rectangles represent the LC blocks).[96] Copyright 2005, Royal Society of Chemistry.

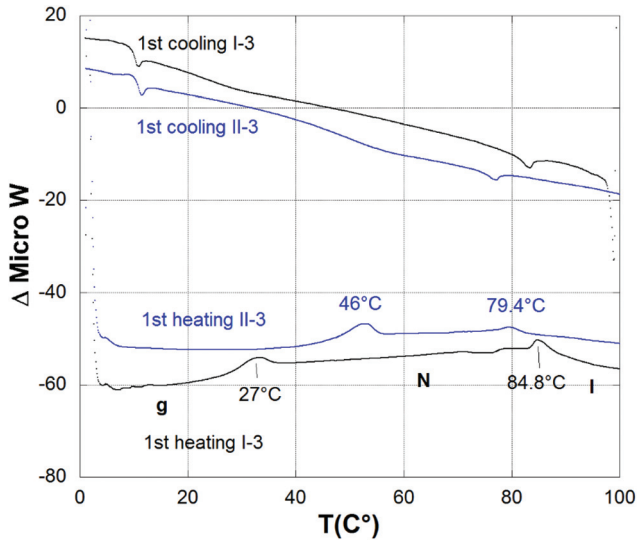

Fig. 17 High sensitivity DSC thermograms of polymersome suspensions of PEG_{45}-*b*-$PA444_7$ (I-3) and PEG_{45}-*b*-$PMAazo444_{12}$ (II-3).[106] Copyright 2011, Royal Society of Chemistry.

Giant polymersomes (>10 μm in diameter) were prepared first by the method of inverted emulsion from the azobenzene-containing block copolymer PEG-*b*-PMAazoA444 in order to follow the morphological changes of the polymersomes under an optical microscope.[111] Fig. 18c shows the morphological evolution of PEG-*b*-PMAazoA444 polymersome under UV illumination. After 300 s of illumination, the polymersome does not seem to open, but the membrane wrinkles. The membrane wrinkling can be explained by the increase of its surface area as follows. Starting from a thin, cigar-like shape corresponding to N state, UV irradiation transforms the LC hydrophobic block into a coil, a process being characterized by a contraction of LC blocks perpendicular to the bilayer and an increased molecular area along the bilayer (see Fig. 18b, the polymer volume was supposed to remain constant).

In order to rapidly open the polymersome, the basic idea is then to induce frustration in the polymersome membrane by breaking up the bilayer symmetry. To implement this approach, we prepared asymmetric polymersomes in which each leaflet consisted of a different type of diblock copolymer: one copolymer was insensitive to any remote stimulus (PEG-*b*-PBD, abbreviated as PBD for simplicity), while the hydrophobic moiety of the second copolymer was the photo-sensitive LC polymer PEG-*b*-PMAazo444 (PAzo).[111] Fig. 19a and b show the chemical structures of the two selected copolymers and a cartoon of the LC copolymer conformation in the membrane both in the absence and in the presence of UV light for the polymersome ePBD-iPAzo (external leaflet = PBD and inner leaflet = PAzo). UV illumination leads to an increase in the molecular area of the inner PAzo leaflet, while the area of the external PBD leaflet does not change. Consequently, the net effect in the mesoscopic scale is the creation of spontaneous curvature of the membrane, which triggers membrane rupture and polymersome bursting. Indeed, exposure to UV illumination around 360 nm caused vesicle rupture, which was completed in less than a few hundreds of milliseconds and the release of the substance from the interior compartment (Fig. 19d). Rapid pore opening (probably *via* heterogeneous pore nucleation, *e.g.*, on a defect) was accompanied by the formation of an outward curling rim, as expected to be generated by the change of spontaneous curvature in the membrane where the inner leaflet is photo-responsive (Fig. 19c). Polymersome bursting also takes place if the inner leaflet is inert and the external leaflet is photo-responsive, but with an inward curling rim during vesicle opening. These results highlight a new general strategy to create stimuli-responsive polymersomes based on the fabrication of asymmetric membranes and driven by a change in membrane spontaneous curvature.

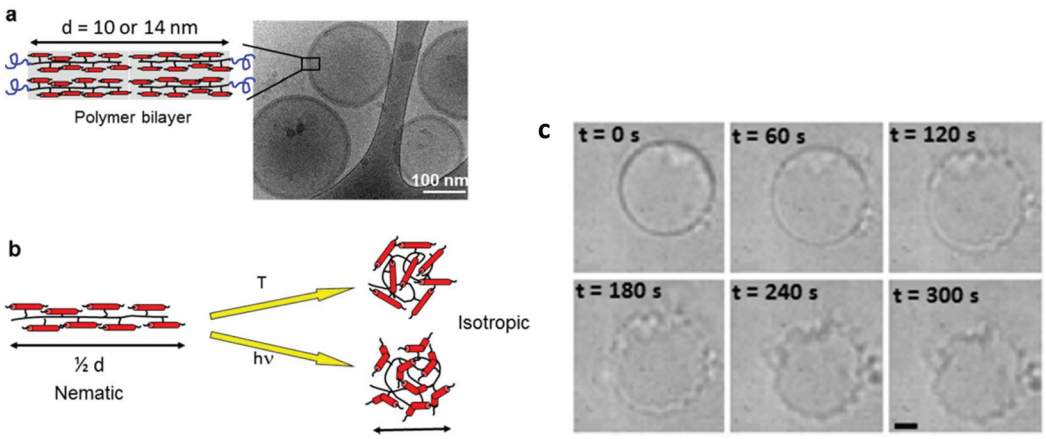

Fig. 18 (a) Schematic representation of the molecular organisation of side-on nematic polymers in the bilayer membrane of polymersomes of PEG-*b*-PA444 and PEG-*b*-PMAazo444 (cryo-EM of polymersomes at the right). (b) The conformational change from a cigar-like shape to a coil of the side-on nematic polymer induced by a nematic–isotropic (N–I) phase transition. This N–I transition can be triggered either by a temperature variation (T) or by a photo-chemical isomerisation of azobenzene under UV illumination ($h\nu$). (c) Membrane wrinkling of a PEG-*b*-PMAazo444 giant polymersome under UV illumination. Scale bar = 10 μm.[111]

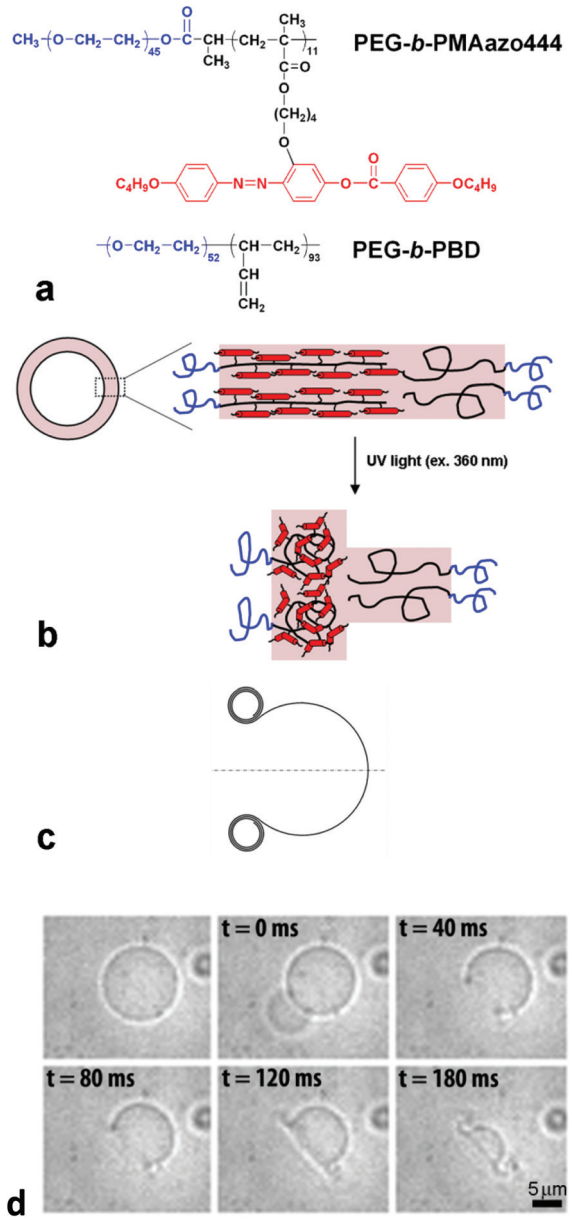

Fig. 19 Copolymers and bilayer conformation. (a) Chemical structures of the two selected copolymers, PEG-*b*-PBD and PEG-*b*-PMAzo444. (b) Cartoon of a polymersome depicting the conformation of both copolymers within the bilayer for an ePBD-iPAzo vesicle. The PEG-*b*-PBD copolymer is always in a coil–coil state. In the absence of UV light, the hydrophobic LC block of the PEG-*b*-PMAzo444 copolymer has a rod-like conformation (corresponding to a nematic state). Under UV illumination, isomerisation of the mesogenic groups induces a conformational change of the polymer backbone to a disordered, isotropic state. The net effect of UV exposure is two-fold: at the molecular scale, the projected area of the LC block is increased; at the mesoscopic scale, the spontaneous curvature of the bilayer is increased. (c) Schematic representation of pore opening driven by outward curling (for ePBD-iPAzo). (d) Snapshots of asymmetrical ePBD-iPAzo polymersome bursting under UV illumination. Bright-field images were taken using a high-speed digital camera. The first image shows the vesicle prior to illumination. Time t = 0 corresponds to pore nucleation. The expulsion of the sucrose solution is visible as the pore nucleated. The other images correspond to pore growth and clearly show outward spirals (scale bar = 5 μm).[111]

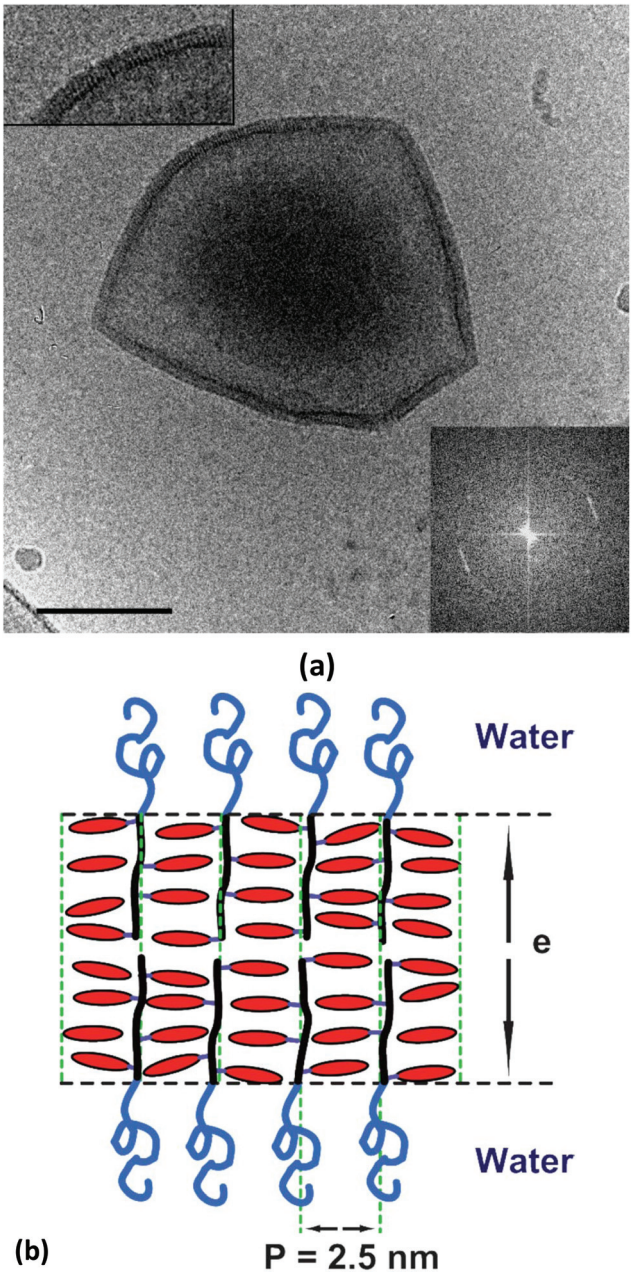

Fig. 20 (a) Cryo-EM images of polymer vesicles of PEG_{45}-*b*-$PA6ester1_{20}$. The inset at the top left is a zoom-in of the upper left area of the vesicle in order to highlight the smectic stripes. The inset at the bottom right is the Fourier transform of the image, diffraction spots corresponding to a period of $P = 2.5 \pm 0.1$ nm. Scale bar = 100 nm. (b) Schematic representation of the smectic molecular organisation within the cross section of the membrane. The hydrophilic PEG in blue connected to the hydrophobic side-chain LC polymer which itself consists of a black backbone and red LC mesogens represented by small elongated ellipsoids. The smectic A structure is a one-layer antiparallel packing (SmA_1). The membrane thickness e is about 10 nm.[99] Copyright 2009, Royal Society of Chemistry.

4.3. Smectic LC polymersomes

Amphiphilic block copolymers with smectic LC blocks, PEG-*b*-PA6ester1 and PEG-*b*-PAChol, can also form polymersomes using a typical nanoprecipitation method. However, both polymersomes are not classical spherical vesicles. What is more striking here is that the copolymers PEG-*b*-PA6ester1 form faceted vesicles, while the copolymers PEG-*b*-PAChol form ellipsoidal vesicles.

Faceted polymersomes of PEG_{45}-*b*-$PA6ester1_{20}$ are shown in Fig. 20a.[99] Periodic stripes perpendicular to the membrane surface are clearly visible. Their period was found to be 2.5 nm, in agreement with the period of the SmA_1 phase (the subscript number 1 means the period corresponds to the length of one mesogen) in the pure state of the homopolymer PA6ester1 (see Fig. 20b for the mesogen organisation). The membrane thickness is e = 10 nm, showing a rather stretched backbone in the bilayer membrane.

The polymersomes of PEG_{45}-*b*-$PAChol_{10}$ and PEG_{45}-*b*-$PAChol_{16}$ are ellipsoidal.[97] Fig. 21 shows their cryo-EM images: some of them have smooth tips (Fig. 21a and b), and others have spherical buds emanating from the poles (Fig. 21b). Periodic stripes are clearly present in a large part of the membrane except in the two extremities of the polymersome. Spherical buds or smooth tips are isotropic. The stripes' period was found to be P = 4.30 nm, corresponding to the layer spacing of interdigitated smectic A phase of PAChol in the pure state (denoted as SmA_d, the subscript letter d means two mesogens interdigitate to make a smectic layer). Fig. 21c shows a schematic representation of the mesogen organisation of SmA_d within the cross section of the membrane parallel to the major axis of ellipsoidal vesicles. The membrane thickness turned out to be substantially different in smectic regions and isotropic regions. For PEG_{45}-*b*-$PAChol_{10}$, the thickness falls in the range e = 8–13 nm in smectic regions but is thinner in the buds where no stripes are visible (in the range e_I = 4–7 nm). For PEG_{45}-*b*-$PAChol_{16}$, the corresponding thicknesses are e = 10–13 nm and e_I = 5–7 nm. The LC polymer membranes possess both liquid crystal and polymer characteristics, which should be taken into account at the same time when analysing the morphology of LC polymersomes. On the one hand, bending of the membrane parallel to the smectic layer does

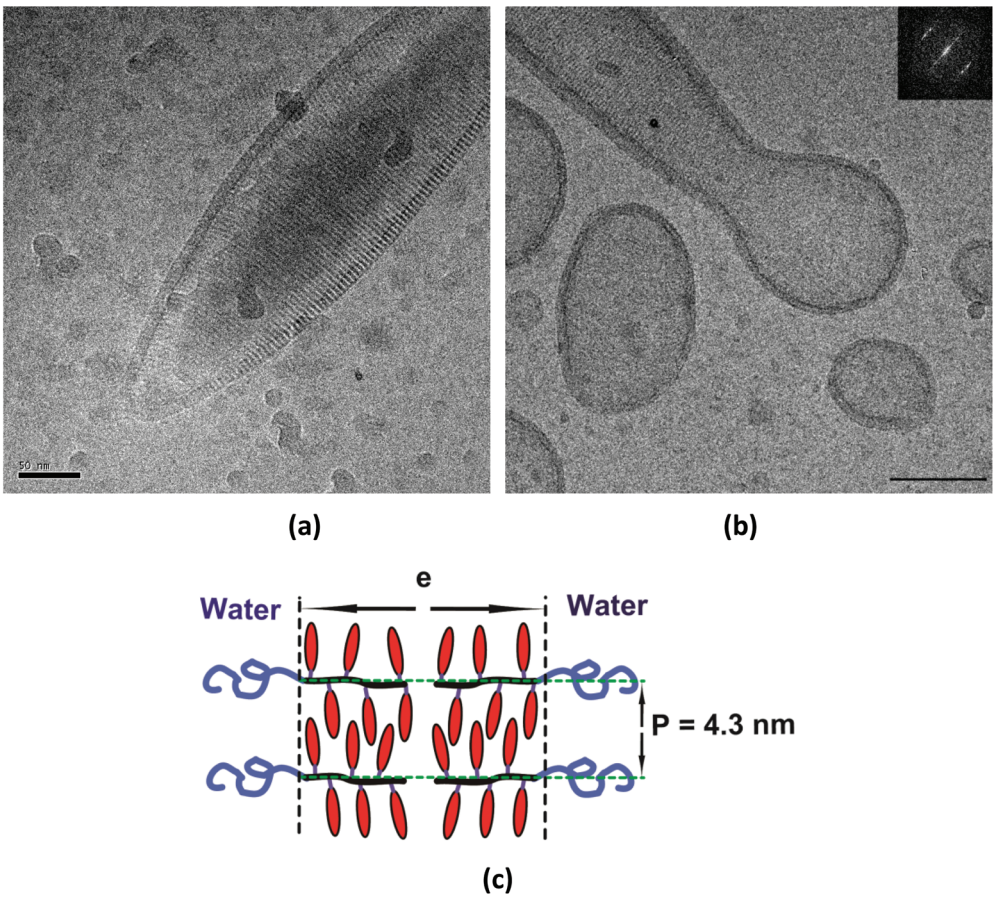

Fig. 21 Cryo-EM images of smectic polymer vesicles of PEG-*b*-PAChol. (a) PEG_{45}-*b*-$PAChol_{16}$, scale bar = 50 nm. (b) PEG_{45}-*b*-$PAChol_{10}$, scale bar = 100 nm. The inset in (b) is the Fourier transform of the upper left area of the vesicles. The periodicity of all smectic areas is identical and corresponds to P = 4.3 ± 0.1 nm. The buds of the vesicles in (b) are not liquid crystalline as seen on the Fourier transform (not shown). (c) Schematic representation of the smectic molecular organisation within the cross section of the membrane parallel to the major axis.[97] Copyright 2009, Royal Society of Chemistry.

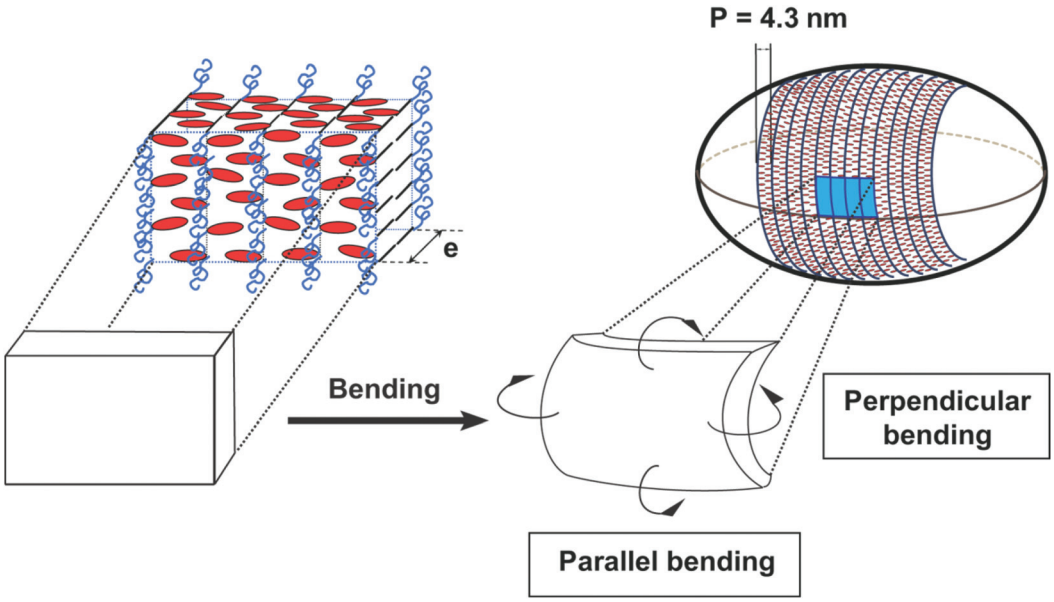

Fig. 22 Schematic representation of a smectic ellipsoidal polymer vesicle. *e* is the membrane thickness and *P* is the smectic period.[97] Copyright 2009, Royal Society of Chemistry.

not change the layer spacing, while bending perpendicular to the layers makes the layer spacing on both sides of the membrane unequal, and therefore costs extra elastic free energy. This explains why the stripes are always perpendicular to the major axis of ellipsoidal vesicles (see Fig. 22 for illustration). On the other hand, bending a membrane with longer polymer chains and with more mesogens should be more energy-consuming than for a membrane with shorter polymer chains and fewer mesogens. That is why PEG_{45}-*b*-$PAChol_{16}$ vesicles are on average larger (with smaller membrane curvature) than PEG_{45}-*b*-$PAChol_{10}$ vesicles. For a much longer copolymer, PEG_{114}-*b*-$PAChol_{60}$, bending perpendicular to the layers becomes even impossible under some conditions. Consequently, long nanotubes instead of ellipsoidal vesicles were obtained.[112]

Another interesting point in the ellipsoidal smectic polymersomes is the special topological defects.[97] Since the smectic order is confined in the two-dimensional membrane, smectic layers (stripes) on a surface with spherical topology must exhibit orientational defects of total charge +2,[113–115] as required by the Gauss–Bonnet–Poincaré theorem. For the polymer vesicles discussed here, since all the smectic layers are roughly perpendicular to the major axis and each polar region should carry disclination charge +1. Moreover, it is proposed that all stripes should generically form helices around the major axis, because the special case where all smectic layers form closed circles is possible but unlikely. Consequently, the +1 disclinations around each pole are more appropriately characterised as tightly bound pairs of +1/2 disclinations, as illustrated in Fig. 23. These topological defects could also be the nucleator of vesicle budding and result in spherical isotropic buds that relieve also topological constraints. The budding phenomenon is, therefore, a result of smectic–isotropic phase separation (see ref. 97 for the theoretical analysis of the necks of buds).

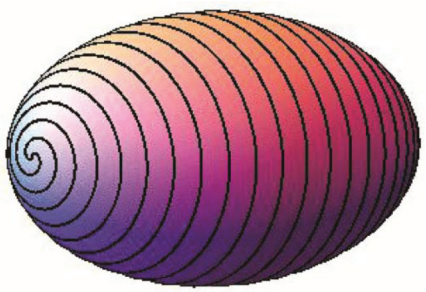

Fig. 23 Expected defect structure at a pole of a smectic ellipsoidal polymer vesicle.[97] Copyright 2009, Royal Society of Chemistry.

On analysing all these faceted and ellipsoidal polymersomes, Xing *et al.* have developed a more complete theoretical model to explain the morphology of polymersomes with LC orders in the membrane.[116] The morphology of a bilayer is controlled by the competition between the bending energy of the polymer bilayer and the Frank free energy of the LC structure. Using both analytic and numerical approaches, it was shown that the possible low free energy morphologies include nanosize cylindrical micelles (nanofibres), faceted tetrahedral vesicles, and ellipsoidal vesicles, as well as cylindrical vesicles (nanotubes). Two limiting cases were considered: $K \ll \kappa$ and $K \gg \kappa$ (K is the Frank constant and κ the bending rigidity). In the case of $K \ll \kappa$, the dominant contribution to the total energy is then the bending energy: minimizing this leads to a round spherical shape. However, as the bending energy is not isotropic, the shape will reflect the anisotropy of the bending

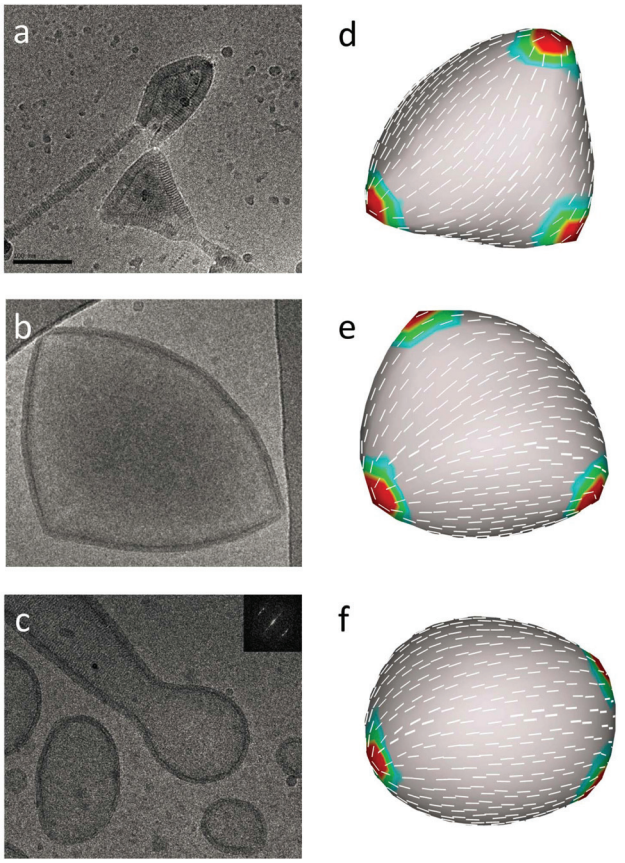

Fig. 24 Comparison between experimental observations (a)–(c) and computer simulations (d)–(f). Left: Experimental results: (a) a tetrahedral smectic vesicle; (b) a fat tetrahedral smectic vesicle; (c) an ellipsoidal smectic vesicle. Right: Simulation results for the case of $K_3/K_1 \approx 2.0$, (d) $\kappa = 0.04$; (e) $\kappa = 0.1$; (f) $\kappa = 0.5$. The contour plots show the distribution of the local Frank free energy. K_3 and K_1 are splay and bend Frank constants, respectively.[116]

moduli, leading to ellipsoidal shapes, as observed experimentally and discussed above. In the case of $K > \kappa$, the system should first minimize the Frank free energy: the ground state morphology of a vesicle with spherical topology is a faceted tetrahedron, with a strength disclination located at each of the four corners. This structure was indeed observed in our experiments,[99,112] as well as in the simulation (Fig. 24).

We speculate that the edges and the vertices in faceted LC polymersomes, the isotropic buds and the disclinations of tips in ellipsoidal LC polymersomes could be used as interesting stimuli-responsive release sites as in the crystalline liposomes.

5. Summary and outlook

We have described in this paper the structures and morphologies of liposomes and polymersomes with crystalline and liquid crystalline phases inside their membranes. Representative liposomes and polymersomes discussed are summarized in Table 1. Any structural and morphological changes based on phase transitions and phase boundary changes can be used to make stimuli-responsive systems, which are exciting candidates as new smart drug delivery systems. These vesicles are responsive to physical stimuli, such as temperature variation, shear stress, light illumination, magnetic fields and electric fields, which have numerous advantages over chemical stimuli because they could be applied locally, remotely and rapidly, and also because there is no modification of chemical environment caused by additional reagents.

Crystalline liposomes and polymersomes have a common feature: the vesicles do not present a smooth spherical shape but a faceted shape. This is because the curved geometry is incommensurable with crystals having three-dimensional translational symmetry. On the one hand, these vesicles show increased permeability around the T_m because of the formation of crystalline grain boundaries and the pre-melting occurring at these boundaries. On the other hand, the faceted vesicles are often mechanically weak and sensitive to shear stress. As vesicles should be robust and stealthy before reaching targeted sites, polymersomes and polymer-coated (*e.g.*, PEGylated) liposomes with crystalline phases show obvious advantages over simple liposomes. Crystalsomes based on single crystal-like homopolymers exhibiting a 100 to 1000 times higher bending modulus than that of conventional polymersomes could be a promising system for drug delivery if stimuli-responsive structure tuning could be introduced.

Liquid crystalline polymersomes, made of LC amphiphilic block copolymers with a variety of chemical structures and mesophorphic phases, show also great potential in developing unique stimuli-responsive encapsulation and delivery systems. An example of light-stimulated bursting of LC polymersomes has been highlighted in this paper. More efforts on studies of LC polymersomes will be necessary for their future applications, for example, developing LC polymersomes sensitive to *in vivo* stimuli,[18] or making LC polymersomes biocomptible and biodegradable.[117]

The thermo-sensitive anti-cancer drug ThermoDox®[118] based on crystalline liposomes[19] has been evaluated in a global phase III clinical study since 2014. It may hopefully appear in the market in the very near future. However, the physical phenomena behind this nano-carrier were discovered and described much earlier. The physics of the 2D crystalline-to-isotropic phase transition was first described in 1973.[119] The crystalline–isotropic grain boundary model was established in 1987.[120,121] The lysolipid-containing thermal-sensitive liposome was discovered in 1999.[25] From the fundamental research on the lipid phase transition to ThermoDox®, about 40 years have passed with tireless efforts from scientists. As the research on polymersomes started only around 2000,[1] we should be confident that on the horizon of 2040 or earlier, smart nano-drugs or nano-bioimaging agents based on polymersomes could see the light of day.

Table 1 Representative liposomes and polymersomes described in the article

Vesicles	Composition	Structure	Responsive feature	Potential application	Ref.
ThermoDox® liposomes	DPPC (86%), MPPC (10%) and PEG2000-DSPE (4%)	Football-like structure	Rapid and complete drug release upon the increase of temperature (41–42 °C)	Thermo-sensitive carriers for anti-cancer drugs	25 and 27
Catanionic vesicles	$C_{13}COOH$ + CTAOH (*e.g.* with a ratio of 1 : 2)	Regular hollow icosahedron	Potentially responsive to shear stress with holes and faceted structure	Possible shear stress sensitive nano-vehicle under salt-free conditions	55
Shear stress sensitive vesicles	Pad-PC-Pad or Pad-Pad-PC	Faceted vesicle	Disruption upon increased shear stress (*e.g.* in constricted vessels)	Shear stress sensitive drug carriers to treat cardiovascular disease	70, 72 and 76
Crystalline polymersomes	PTMC-*b*-PGA	Spherical polymersome with semi-crystalline membrane	Higher drug release rate with higher temperature	Thermo-sensitive drug carriers	21 and 89
	PEO-*b*-(PODMA-*co*-PDSMA)	Bicontinuous or multilamellar polymersome with semi-crystalline membrane	Significantly enhanced release rate upon crystalline melting in the membrane	Thermo-sensitive drug carriers with a tuneable melting temperature	92
Crystalsomes	PLLA or PE	Capsule with single-crystal-like phase formed by homopolymers	Potentially responsive to heating stimulation	Thermo-sensitive drug carriers	93 and 94
	Polyurea	Capsule with semi-crystalline phase formed by *in situ* synthesized homopolymers	Higher drug release rate with lower crystallinity	Thermo-sensitive drug carriers	95
Liquid crystal polymersomes	AA-BB-AA	Polymersome with liquid crystal blocks (BB) in the membrane	Nanoscale vesicles turn into micrometer-scale vesicles under an electric field	Electric field responsive drug carriers	105
	PEG-*b*-PMAazo444 (PAzo) and PEG-*b*-PBD (PBD)	Spherical polymersome with an asymmetric structure of bilayer membrane (ePBD-iPAzo or iPBD-ePAzo)	Rapid opening with outward or inward curling upon UV illumination (360 nm)	Photo-responsive drug carriers	111
	PEG-*b*-PA6ester1	Faceted vesicle with smectic structure in the membrane	Potentially responsive to shear stress	Possible shear stress sensitive drug carriers	99
	PEG-*b*-PAChol	Ellipsoidal vesicle with smectic structure in the membrane	Possible morphological changes upon heating	Possible thermo-responsive drug carriers	97

Conflicts of interest

There are no conflicts to declare.

Acknowledgements

We acknowledge the French National Research Agency (project ANR-16-CE29-0028) and the National Natural Science Foundation of China (project 21528402) for financial support. Yangwei Deng thanks the China Scholarship Council for funding his PhD scholarship in France.

References

1 B. M. Discher, Y. Y. Won, D. S. Ege, J. C. M. Lee, F. S. Bates, D. E. Discher and D. A. Hammer, *Science*, 1999, **284**, 1143–1146.
2 D. E. Discher and A. Eisenberg, *Science*, 2002, **297**, 967–973.
3 D. E. Discher and F. Ahmed, *Annu. Rev. Biomed. Eng.*, 2006, **8**, 323–341.
4 V. P. Torchilin, *Nat. Rev. Drug Discovery*, 2005, **4**, 145–160.
5 P. J. Photos, L. Bacakova, B. Discher, F. S. Bates and D. E. Discher, *J. Controlled Release*, 2003, **90**, 323–334.
6 J. S. Lee and J. Feijen, *J. Controlled Release*, 2012, **158**, 312–318.
7 C. LoPresti, H. Lomas, M. Massignani, T. Smart and G. Battaglia, *J. Mater. Chem.*, 2009, **19**, 3576–3590.
8 P. P. Ghoroghchian, P. R. Frail, K. Susumu, D. Blessington, A. K. Brannan, F. S. Bates, B. Chance, D. A. Hammer and M. J. Therien, *Proc. Natl. Acad. Sci. U. S. A.*, 2005, **102**, 2922–2927.
9 D. H. Levine, P. P. Ghoroghchian, J. Freudenberg, G. Zhang, M. J. Therien, M. I. Greene, D. A. Hammer and R. Murali, *Methods*, 2008, **46**, 25–32.
10 P. P. Deshpande, S. Biswas and V. P. Torchilin, *Nanomedicine*, 2013, **8**, 1509–1528.
11 F. H. Meng, Z. Y. Zhong and J. Feijen, *Biomacromolecules*, 2009, **10**, 197–209.
12 J. Z. Du and R. K. O'Reilly, *Soft Matter*, 2009, **5**, 3544–3561.
13 M.-H. Li and P. Keller, *Soft Matter*, 2009, **5**, 927–937.
14 K. T. Kim, S. A. Meeuwissen, R. J. M. Nolte and J. C. M. van Hest, *Nanoscale*, 2010, **2**, 844–858.

15 K. Dan and S. Ghosh, *Angew. Chem., Int. Ed.*, 2013, **52**, 7300–7305.
16 D. Grafe, J. Gaitzsch, D. Appelhans and B. Voit, *Nanoscale*, 2014, **6**, 10752–10761.
17 M. A. Yassin, D. Appelhans, R. Wiedemuth, P. Formanek, S. Boye, A. Lederer, A. Temme and B. Voit, *Small*, 2015, **11**, 1580–1591.
18 L. Jia, D. Cui, J. Bignon, A. Di Cicco, J. Wdzieczak-Bakala, J. Liu and M.-H. Li, *Biomacromolecules*, 2014, **15**, 2206–2217.
19 D. Needham, *Patent US* 6200598B1, 2002.
20 R. Lencioni and D. Cioni, *Hep. Oncol.*, 2016, **3**, 193–200.
21 C. Sanson, J. F. Le Meins, C. Schatz, A. Soum and S. Lecommandoux, *Soft Matter*, 2010, **6**, 1722–1730.
22 L. Jia and M.-H. Li, *Liq. Cryst.*, 2014, **41**, 368–384.
23 A. H. Groschel and A. H. E. Mueller, *Nanoscale*, 2015, **7**, 11841–11876.
24 D. Wu, Y. Huang, F. Xu, Y. Mai and D. Yan, *J. Polym. Sci., Part A: Polym. Chem.*, 2017, **55**, 1459–1477.
25 G. R. Anyarambhatla and D. Needham, *J. Liposome Res.*, 1999, **9**, 491–506.
26 S. Leekumjorn and A. K. Sum, *Biochim. Biophys. Acta*, 2007, **1768**, 354–365.
27 D. Needham and M. W. Dewhirst, *Adv. Drug Delivery Rev.*, 2001, **53**, 285–305.
28 W. V. Kraske and D. B. Mountcastle, *Biochim. Biophys. Acta, Biomembr.*, 2001, **1514**, 159–164.
29 M. B. Yatvin, J. N. Weinstein, W. H. Dennis and R. Blumenthal, *Science*, 1978, **202**, 1290–1293.
30 T. L. Andresen, S. S. Jensen and K. Jorgensen, *Prog. Lipid Res.*, 2005, **44**, 68–97.
31 P. Pradhan, J. Giri, F. Rieken, C. Koch, O. Mykhaylyk, M. Doblinger, R. Banerjee, D. Bahadur and C. Plank, *J. Controlled Release*, 2010, **142**, 108–121.
32 L. Hosta-Rigau, Y. Zhang, B. M. Teo, A. Postma and B. Staedler, *Nanoscale*, 2013, **5**, 89–109.
33 D. Volodkin, H. Mohwald, J. C. Voegel and V. Ball, *J. Controlled Release*, 2007, **117**, 111–120.
34 S. T. Hyde, *J. Phys.*, 1990, **51**, 7209–7228.
35 D. Needham, G. Anyarambhatla, G. Kong and M. W. Dewhirst, *Cancer Res.*, 2000, **60**, 1197–1201.
36 B. J. Wood, R. T. Poon, J. K. Locklin, M. R. Dreher, K. K. Ng, M. Eugeni, G. Seidel, S. Dromi, Z. Neennan, M. Kolf, C. D. V. Black, R. Prabhakar and S. K. Libutti, *J. Vasc. Interv. Radiol.*, 2012, **23**, 248–255.
37 T. M. Zagar, Z. Vujaskovic, S. Formenti, H. Rugo, F. Muggia, B. O'Connor, R. Myerson, P. Stauffer, I. C. Hsu, C. Diederich, W. Straube, M. K. Boss, A. Boico, O. Craciunescu, P. Maccarini, D. Needham, N. Borys, K. L. Blackwell and M. W. Dewhirst, *Int. J. Hyperthermia*, 2014, **30**, 285–294.
38 P. C. Lyon, L. F. Griffiths, J. Lee, D. Chung, R. Carlisle, F. Wu, M. R. Middleton, F. V. Gleeson and C. C. Coussios, *J. Ther. Ultrasound*, 2017, **5**, 28.
39 A. A. Manzoor, L. H. Lindner, C. D. Landon, J.-Y. Park, A. J. Simnick, M. R. Dreher, S. Das, G. Hanna, W. Park, A. Chilkoti, G. A. Koning, T. L. M. ten Hagen, D. Needham and M. W. Dewhirst, *Cancer Res.*, 2012, **72**, 5566–5575.
40 G. Kong, G. Anyarambhatla, W. P. Petros, R. D. Braun, O. M. Colvin, D. Needham and M. W. Dewhirst, *Cancer Res.*, 2000, **60**, 6950–6957.
41 ClinicalTrials.gov, Study of ThermoDox With Standardized Radiofrequency Ablation (RFA) for Treatment of Hepatocellular Carcinoma (HCC) (OPTIMA). https://clinicaltrials.gov/ct2/show/study/NCT02112656.
42 ClinicalTrials.gov, Phase 1/2 Study of ThermoDox With Approved Hyperthermia in Treatment of Breast Cancer Recurrence at the Chest Wall (DIGNITY). https://clinicaltrials.gov/ct2/show/study/NCT00826085.
43 ClinicalTrial.gov, Targeted Chemotherapy Using Focused Ultrasound for Liver Tumours (TARDOX). https://clinicaltrials.gov/ct2/show/study/NCT02181075.
44 Y. Dou, K. Hynynen and C. Allen, *J. Controlled Release*, 2017, **249**, 63–73.
45 T. Tagami, M. J. Ernsting and S.-D. Li, *J. Controlled Release*, 2011, **152**, 303–309.
46 M. Hossann, M. Wiggenhorn, A. Schwerdt, K. Wachholz, N. Teichert, H. Eibl, R. D. Issels and L. H. Lindner, *Biochim. Biophys. Acta, Biomembr.*, 2007, **1768**, 2491–2499.
47 M. Dunne, K. Hynynen and C. Allen, *Nano Today*, 2017, **16**, 9–13.
48 N. Du, R. Y. Song, H. S. Zhang, J. C. Sun, S. L. Yuan, R. J. Zhang and W. G. Hou, *Colloids Surf., A*, 2016, **509**, 195–202.
49 J. J. Panda and V. S. Chauhan, *Polym. Chem.*, 2014, **5**, 4418–4436.
50 J. C. Hao and T. Zemb, *Curr. Opin. Colloid Interface Sci.*, 2007, **12**, 129–137.
51 S. S. Hao, Q. Y. Zhai, L. Zhao and B. C. Xu, *Colloids Surf., A*, 2016, **509**, 116–122.
52 A. L. Fameau and T. Zemb, *Adv. Colloid Interface Sci.*, 2013, **207**, 43–64.
53 J. C. Hao and H. Hoffmann, *Curr. Opin. Colloid Interface Sci.*, 2004, **9**, 279–293.
54 T. Zemb, M. Dubois, B. Deme and T. Gulik-Krzywicki, *Science*, 1999, **283**, 816–819.
55 M. Dubois, B. Deme, T. Gulik-Krzywicki, J. C. Dedieu, C. Vautrin, S. Desert, E. Perez and T. Zemb, *Nature*, 2001, **411**, 672–675.
56 M. Dubois, V. Lizunov, A. Meister, T. Gulik-Krzywicki, J. M. Verbavatz, E. Perez, J. Zimmerberg and T. Zemb, *Proc. Natl. Acad. Sci. U. S. A.*, 2004, **101**, 15082–15087.
57 M. A. Hartmann, R. Weinkamer, T. Zemb, F. D. Fischer and P. Fratzl, *Phys. Rev. Lett.*, 2006, **97**, 18106.
58 G. Vernizzi and M. O. de la Cruz, *Proc. Natl. Acad. Sci. U. S. A.*, 2007, **104**, 18382–18386.
59 G. Vernizzi, D. S. Zhang and M. O. de la Cruz, *Soft Matter*, 2011, **7**, 6285–6293.
60 M. A. Greenfield, L. C. Palmer, G. Vernizzi, M. O. de la Cruz and S. I. Stupp, *J. Am. Chem. Soc.*, 2009, **131**, 12030–12031.

61 N. Delorme, J. F. Bardeau, D. Carriere, M. Dubois, A. Gourbil, H. Mohwald, T. Zemb and A. Fery, *J. Phys. Chem. B*, 2007, **111**, 2503–2505.
62 C. A. Haselwandter and R. Phillips, *Phys. Rev. Lett.*, 2010, **105**, 228101.
63 C. Y. Leung, L. C. Palmer, S. Kewalramani, B. F. Qiao, S. I. Stupp, M. O. de la Cruz and M. J. Bedzyk, *Proc. Natl. Acad. Sci. U. S. A.*, 2013, **110**, 16309–16314.
64 I. A. Fedotenko, P. L. Zaffalon, F. Favarger and A. Zumbuehl, *Tetrahedron Lett.*, 2010, **51**, 5382–5384.
65 H. P. Liu, Z. Zhu, H. Z. Kang, Y. R. Wu, K. Sefan and W. H. Tan, *Chem. – Eur. J.*, 2010, **16**, 3791–3797.
66 G. H. Dehaas, R. Dijkman, M. G. Vanoort and R. Verger, *Biochim. Biophys. Acta*, 1990, **1043**, 75–82.
67 C. H. Jia and A. H. Haines, *J. Chem. Soc., Perkin Trans. 1*, 1993, 2521–2523.
68 J. Sunamoto, M. Goto, K. Iwamoto, H. Kondo and T. Sato, *Biochim. Biophys. Acta*, 1990, **1024**, 209–219.
69 C. M. Gupta and A. Bali, *Biochim. Biophys. Acta*, 1981, **663**, 506–515.
70 R. Tanasescu, M. A. Lanz, D. Mueller, S. Tassler, T. Ishikawa, R. Reiter, G. Brezesinski and A. Zumbuehl, *Langmuir*, 2016, **32**, 4896–4903.
71 A. Weinberger, R. Tanasescu, C. Stefaniu, L. A. Fedotenko, F. Favarger, T. Ishikawa, G. Brezesinski, C. M. Marques and A. Zumbuehl, *Langmuir*, 2015, **31**, 1879–1884.
72 M. N. Holme, I. A. Fedotenko, D. Abegg, J. Althaus, L. Babel, F. Favarger, R. Reiter, R. Tanasescu, P. L. Zaffalon, A. Ziegler, B. Muller, T. Saxer and A. Zumbuehl, *Nat. Nanotechnol.*, 2012, **7**, 536–543.
73 T. Saxer, A. Zumbuehl and B. Muller, *Cardiovasc. Res.*, 2013, **99**, 328–333.
74 M. Buscema, S. Matviykiv, T. Meszaros, G. Gerganova, A. Weinberger, U. Mettal, D. Mueller, F. Neuhaus, E. Stalder, T. Ishikawa, R. Urbanics, T. Saxer, T. Pfohl, J. Szebeni, A. Zumbuehl and B. Mueller, *J. Controlled Release*, 2017, **264**, 14–23.
75 L. A. Fedotenko, C. Stefaniu, G. Brezesinski and A. Zumbuehl, *Langmuir*, 2013, **29**, 9428–9435.
76 F. Neuhaus, D. Mueller, R. Tanasescu, S. Balog, T. Ishikawa, G. Brezesinski and A. Zumbuehl, *Angew. Chem., Int. Ed.*, 2017, **56**, 6515–6518.
77 M. Antonietti and S. Forster, *Adv. Mater.*, 2003, **15**, 1323–1333.
78 A. Blanazs, S. P. Armes and A. J. Ryan, *Macromol. Rapid Commun.*, 2009, **30**, 267–277.
79 F. H. Schacher, J. Elbert, S. K. Patra, S. F. Yusoff, M. A. Winnik and I. Manners, *Chem. – Eur. J.*, 2012, **18**, 517–525.
80 K. Rajagopal, A. Mahmud, D. A. Christian, J. D. Pajerowski, A. E. X. Brown, S. M. Loverde and D. E. Discher, *Macromolecules*, 2010, **43**, 9736–9746.
81 H. S. Seung and D. R. Nelson, *Phys. Rev. A*, 1988, **38**, 1005–1018.
82 Y. W. Deng, T. Zou, X. F. Tao, V. Semetey, S. Trepout, S. Marco, J. Ling and M.-H. Li, *Biomacromolecules*, 2015, **16**, 3265–3274.
83 T. Uneyama, *J. Chem. Phys.*, 2007, **126**, 114902.
84 X. H. He and F. Schmid, *Macromolecules*, 2006, **39**, 2654–2662.
85 J. A. Zupancich, F. S. Bates and M. A. Hillmyer, *Macromolecules*, 2006, **39**, 4286–4288.
86 J. S. Katz, K. A. Eisenbrown, E. D. Johnston, N. P. Kamat, J. Rawson, M. J. Therien, J. A. Burdick and D. A. Hammer, *Soft Matter*, 2012, **8**, 10853–10862.
87 K. J. Zhu, R. W. Hendren, K. Jensen and C. G. Pitt, *Macromolecules*, 1991, **24**, 1736–1740.
88 C. Sanson, C. Schatz, J. F. Le Meins, A. Brulet, A. Soum and S. Lecommandoux, *Langmuir*, 2010, **26**, 2751–2760.
89 C. Sanson, C. Schatz, J. F. Le Meins, A. Soum, J. Thevenot, E. Garanger and S. Lecommandoux, *J. Controlled Release*, 2010, **147**, 428–435.
90 C. Sanson, O. Diou, J. Thevenot, E. Ibarboure, A. Soum, A. Brulet, S. Miraux, E. Thiaudiere, S. Tan, A. Brisson, V. Dupuis, O. Sandre and S. Lecommandoux, *ACS Nano*, 2011, **5**, 1122–1140.
91 D. Bacinello, E. Garanger, D. Taton, K. C. Tam and S. Lecommandoux, *Eur. Polym. J.*, 2015, **62**, 363–373.
92 O. R. Monaghan, P. H. H. Bomans, N. A. J. M. Sommerdijk and S. J. Holder, *Polym. Chem.*, 2017, **8**, 5303–5316.
93 W. Wang, H. Qi, T. Zhou, S. Mei, L. Han, T. Higuchi, H. Jinnai and C. Y. Li, *Nat. Commun.*, 2016, **7**, 10599.
94 W. Wang, M. C. Staub, T. Zhou, D. M. Smith, H. Qi, E. D. Laird, S. Cheng and C. Y. Li, *Nanoscale*, 2017, **10**, 268–276.
95 I. Schlegel, R. Muñoz-Espí, P. Renz, I. Lieberwirth, G. Floudas, Y. Suzuki, D. Crespy and K. Landfester, *Macromolecules*, 2017, **50**, 4725–4732.
96 J. Yang, D. Levy, W. Deng, P. Keller and M.-H. Li, *Chem. Commun.*, 2005, 4345–4347.
97 L. Jia, A. Cao, D. Levy, B. Xu, P. A. Albouy, X. J. Xing, M. J. Bowick and M.-H. Li, *Soft Matter*, 2009, **5**, 3446–3451.
98 J. Yang, R. Pinol, F. Gubellini, D. Levy, P. A. Albouy, P. Keller and M.-H. Li, *Langmuir*, 2006, **22**, 7907–7911.
99 B. Xu, R. Pinol, M. Nono-Djamen, S. Pensec, P. Keller, P. A. Albouy, D. Levy and M.-H. Li, *Faraday Discuss.*, 2009, **143**, 235–250.
100 L. Jia, P. A. Albouy, A. Di Cicco, A. Cao and M.-H. Li, *Polymer*, 2011, **52**, 2565–2575.
101 L. Jia, M. Liu, A. Di Cicco, P. A. Albouy, B. Brissault, J. Penelle, S. Boileau, V. Barbier and M.-H. Li, *Langmuir*, 2012, **28**, 11215–11224.
102 H. Yang, L. Jia, C. H. Zhu, A. Di-Cicco, D. Levy, P. A. Albouy, M.-H. Li and P. Keller, *Macromolecules*, 2010, **43**, 10442–10451.
103 F. Zhou, Z. Zhang, G. Jiang, J. Lu, X. Chen, Y. Li, N. Zhou and X. Zhu, *Polym. Chem.*, 2016, **7**, 2785–2789.

104 C. K. Wong, A. F. Mason, M. H. Stenzel and P. Thordarson, *Nat. Commun.*, 2017, **8**, 1240.
105 S. Honda, M. Koga, M. Tokita, T. Yamamoto and Y. Tezuka, *Polym. Chem.*, 2015, **6**, 4167–4176.
106 S. Hocine, A. Brûlet, L. Jia, J. Yang, A. Di Cicco, L. Bouteiller and M.-H. Li, *Soft Matter*, 2011, **7**, 2613.
107 S. Lecommandoux, M. F. Achard, F. Hardouin, A. Brulet and J. P. Cotton, *Liq. Cryst.*, 1997, **22**, 549–555.
108 J. P. Cotton and F. Hardouin, *Prog. Polym. Sci.*, 1997, **22**, 795–828.
109 M.-H. Li, P. Keller, J. Y. Yang and P. A. Albouy, *Adv. Mater.*, 2004, **16**, 1922–1925.
110 M.-H. Li, P. Keller, B. Li, X. G. Wang and M. Brunet, *Adv. Mater.*, 2003, **15**, 569–572.
111 E. Mabrouk, D. Cuvelier, F. Brochard-Wyart, P. Nassoy and M.-H. Li, *Proc. Natl. Acad. Sci. U. S. A.*, 2009, **106**, 7294–7298.
112 L. Jia, D. Levy, D. Durand, M. Imperor-Clerc, A. Cao and M.-H. Li, *Soft Matter*, 2011, **7**, 7395–7403.
113 T. C. Lubensky and J. Prost, *J. Phys. II*, 1992, **2**, 371–382.
114 X. Xing, *Phys. Rev. Lett.*, 2008, **101**, 147801.
115 D. R. Nelson, *Nano Lett.*, 2002, **2**, 1125–1129.
116 X. Xing, H. Shin, M. J. Bowick, Z. Yao, L. Jia and M.-H. Li, *Proc. Natl. Acad. Sci. U. S. A.*, 2012, **109**, 5202–5206.
117 L. Zhou, D. Zhang, S. Hocine, A. Pilone, S. Trépout, S. Marco, C. Thomas, J. Guo and M.-H. Li, *Polym. Chem.*, 2017, **8**, 4776–4780.
118 Celsion Corporation. In animal models, ThermoDox® has been shown to deliver 25 times more doxorubicin into tumors than does intravenous (IV) infusion alone, and 5 times more doxorubicin than standard liposomal formulations of the drug. http://celsion.com/thermodox/.
119 D. Papahadjopoulos, K. Jacobson, S. Nir and T. Isac, *Biochim. Biophys. Acta*, 1973, **311**, 330–348.
120 O. G. Mouritsen and M. J. Zuckermann, *Phys. Rev. Lett.*, 1987, **58**, 389–392.
121 J. Risbo, K. Jorgensen, M. M. Sperotto and O. G. Mouritsen, *Biochim. Biophys. Acta, Biomembr.*, 1997, **1329**, 85–96.